STUDYING THE MECHANICAL ELEMENTS OF THE TUMOR MICROENVIRONMENT

by

Debonil Maity

A dissertation submitted to Johns Hopkins University in conformity with the requirements

for the degree of Doctor of Philosophy

Baltimore, Maryland

August 2020

ABSTRACT

Extracellular matrices in animal tissue are hydrogels mostly made of collagen. In these matrices, collagen fibers are hierarchically assembled and cross-linked to form a porous and elastic material, through which migrating cells can move by either pushing through open matrix pores, or by actively digesting collagen fibers. The influence of matrix mechanical properties on cell behavior is well studied. Less attention has been focused on hydraulic properties of extracellular matrices, and how hydrodynamic flows in these porous hydrogels are influenced by matrix composition and architecture. Here we study the response of collagen hydrogels using rapid changes in the hydraulic pressure within a microfluidic device, and analyze the data using a poro- elastic theory. Major poro- elastic parameters can be obtained in a single experiment. Results show that depending on the density, porosity, and the degree of geometric confinement, moving micron-sized objects such as cells can experience substantially increased hydraulic resistance when compared to 2D environments.

Furthermore, cells migrating *in vivo* can encounter microenvironments with varying physical properties. One such physical variable is the viscosity of the fluid surrounding the cell. Increased fluid viscosity is expected to increase the hydraulic resistance experienced by the migrating cell and therefore decrease the cell speed. We demonstrate that contrary to this expected result, cells migrate faster in higher viscosity media on 2D substrates. To reveal the molecular mechanism, we examined both actin dynamics and water dynamics driven by ion channel activity. Results show that cells increased in area in high viscosity and acto-myosin dynamics remained similar, except that actin retrograde flow speed is reduced. Inhibiting ion channel fluxes in high viscosity media results in a large reduction in cell speed, suggesting that water flux contributes to the observed speed increase. Moreover, inhibiting cell actin-dependent vesicular trafficking that transports ion channels from the ER to the cell boundary also reduces cell speed in high viscosity media and changes ion channel spatial distribution. Taken together our observations suggest that the cell actin phase and water phase are coupled during cell migration in high viscosity media.

Thesis Advisor: Dr. Sean X. Sun

Thesis Committee: Dr. Konstantinos Konstantopoulos, Dr. Kalina Hristova, Dr. Jamie Spangler (Reader), and Dr. Luo Gu (Reader)

ACKNOWLEDGEMENT

I am really grateful for these amazing five years at Johns Hopkins University where I have matured as a scientist and a thinker. I am no longer a naïve undergraduate with high expectations and through my experience I have understood the flaws in my thought process which also have added a pinch of realism to my expectations. As someone who had a background in Fluid Mechanics from undergraduate research, I am elated to have published articles in Cancer biology which I have always dreamed of, which essentially expanded my repertoire of skill-sets.

I am really thankful to my advisor Dr. Sean X. Sun for being an amazing mentor and showing me how to really focus on a specific problem, despite all the noise and friction that might arise and they are just a part of the journey towards a scientific publication.

I am also really grateful to my friends and family, especially my parents who have been extremely supportive of my research and life beyond research.

Lastly, I really believe that this experience has prepared me for being a good problem solver.

TABLE OF CONTENTS

LIST OF FIGURES

On ***estimation of hydraulic resistance***

On ***a mechanism of cell motility under high hydraulic resistance***

CHAPTER 1: INTRODUCTION ON TUMOR MICROENVIRONMENT

1.1 An Introduction to the mechanical elements of the tumor

The tumor microenvironment (TME) is complex and is composed of various types of cells including resident and infiltrating host cells, secreted factors, extracellular matrix (ECM) proteins. The TME poses various sorts of mechano-chemical cues to not only the cancer cells, but also other cell populations that co-exist. How cancer cells interact with the surrounding cells and the ECM dictates the tumor fate which encompasses tumor eradication, dormant micro-metastases or metastasis to distant organs.

Back in 1863, it was Rudolf Virchow who pioneered the concept that inflammation (characterized by leukocyte infiltration) is a characteristic of solid tumors (Schmidt and Weber 2006). Paget who is considered the pioneer of the TME concept asserted that metastatic colonization is dependent on the properties of the organs (Paget 1989). The TME is now perceived as a dynamic feedback environment, where cancer cells modulate the local microenvironment and interact with the surrounding cells. A dominant component of tumor stroma is fibroblasts that has been shown to make the TME more conducive to cancer progression. Fibroblasts associated with cancer are termed as Carcinoma associated fibroblasts (CAFs), Tumor associated fibroblasts (TAFs). Owing to the fact that fibroblasts are very resilient and have been known to survive severe stress, it is imperative to hypothesize that CAFs may play a dominant role in tumor relapse especially when the TME is subjected to damage induced by chemotherapy or radiotherapy and dynamic remodeling by cancer cells through mechano-chemical feedback mechanism (Kalluri 2016). Some early seminal studies led to the finding that cancer cells recruit normal fibroblasts similar to wound healing process (Durning and Schor 1984). Later studies led to the finding of bio-chemical modes of interaction of cancer cells and fibroblasts which is primarily the transforming growth factor (TGF-β) secreted by cancer cells. PDGF secreted by cancer cells and fibroblasts have also been shown to induce proliferation of fibroblasts and have also been shown to aid cancer progression. It was observed that the ability

of CAFs to aid tumor progression is CAF-derived stromal cell-derived factor 1 (SDF1 or CXCL12) (Kalluri 2016).

Another key biochemical factor that has been studied in detail is hypoxia. Hypoxia is a situation where the tumor cells are deprived of oxygen (which is termed as 'oxygen tension'). It results in increased production of Hypoxia inducible factor (HIF-1). Cellular responses to hypoxia mediated by overexpression of HIF-1α and HIF-2α subunits and their downstream targets has been shown to result in a) increased blood vessel formation, b) aggressiveness of metastatic potential, and c) resistance to therapy (Muz et al. 2015). Stabilization and activity of HIF-α stabilization is known to be governed by epigenetic changes and mutations, which lead to a loss of tumor-suppressors (p53, ING4, and PTEN) and a gain of oncogenes (Ras, Src, Myc, and mTOR) (Kilic-Eren, Boylu, and Tabor 2013; van Uden, Kenneth, and Rocha 2008). The HIF-pathway has been shown to aid tumor growth by a) promoting angiogenesis via Vascular endothelial growth factor (VEGF) and SDF1, b) regulating cell apoptosis and cell survival via BNIP-3, p53, TGF-β, and basic fibroblast growth factor and c) metabolism via regulation of GLUT-1, 3, and glycolytic enzymes (An et al. 1998; Guo et al. 2001; Iliopoulos et al. 1996; Iyer et al. 1998; Roberts et al. 2009; Gregg L Semenza 2013; Siemeister et al. 1996; Zagzag et al. 2005). More specifically, HIF-α contributes to cancer metastasis by altering cancer cell adhesion and migration ability through regulating epithelial-to-mesenchymal transition (EMT), E-cadherin, and regulating expression levels of ZEB1, CXCR4, TCF3, CAIX, Lysyl Oxidase (LOX), MMP-2/ 9 (Azab et al. 2012; Erler et al. 2006; Grabmaier et al. 2004; Krishnamachary et al. 2003, 2006; Staller et al. 2003). As far as stromal cells are concerned, hypoxia has been shown to induce them to produce factors like Angiopoietin-2, Angiopoietin-like 4, platelet-derived growth factor, VEGF, SDF-1 and LOX, ultimately influencing Endothelial cells and Endothelial Progenitor cells which promotes angiogenesis (G L Semenza 2013). Hypoxia also has been shown to demonstrate immunomodulatory and immunosuppressive behavior in that it results in decreased sensitivity to T cell and Natural Killer (NK) cell mediated killing and promoting suppressive cells like regulatory T cells and tumor-associated macrophages, which block effector cells (Siemens et al. 2008; Sitkovsky 2009).

More recently, the influence of the mechanical elements of the tumor have gained attention. The ECM forms the core of the TME and the variation in ECM properties such as rigidity, porosity, insolubility, spatial arrangement and orientation has been shown to be associated with tumor progression (Mierke 2019). Specifically, breast tumorigenesis was found to be accompanied by ECM crosslinking, stiffening and increased focal adhesions, which led to enhanced PI3 kinase activity and invasiveness (Levental et al. 2009). CAFs have been shown to influence ECM stiffness at primary tumors, enhancing cancer cell invasion, and more interestingly, generate ECM tracks to guide cancer cell invasion (Gaggioli et al. 2007). In a comprehensive publication, it was found that cancer cell invasiveness is essentially a complex interplay between cell adhesions, actomyosin-driven contractility and the physical characteristics of the ECM (Ahmadzadeh et al. 2017). Here it was shown that cellular contractility, which leads to matrix fiber realignment, ultimately results in strain stiffening of the ECM. This strain stiffening enables the cells to polarize and develop contractile forces that aid invasion (Ahmadzadeh et al. 2017). Local mechanical stresses have also been implicated with cancer cell invasiveness (Boghaert et al. 2012), in that regions of high invasiveness were correlated with high endogenous mechanical stress. Cells experience diverse microenvironments while migrating through the complex TME. Specifically, they face 3D longitudinal tracks bordering 2D interfaces, such as tracks formed between adjacent bundled collagen fibers and fibrillar interstitial tissues(Stroka et al. 2014) in a TME. It was discovered that cells use water permeation (or “Osmotic Engine”) mode of migration, mediated through ion-exchangers and Aquaporins (AQPs) to navigate through these microenvironments (Stroka et al. 2014). Interestingly, it was observed that cells continued to migrate through these confinements even after actin polymerization was inhibited. While those tracks present a different microenvironment, those environments do contribute to the increase of the extracellular hydraulic resistance (ECHR) experienced by the cells (Li et al. 2019; Li and Sun 2018; Debonil Maity et al. 2019; Zhao et al. 2019). ECHR can be mediated by the geometry of the moving object (here, cells), the cross-sectional size/ length of the confinement, ECM physical property (Debonil Maity et al. 2019) and the viscosity of the surrounding fluid (Li et al. 2019; Li and Sun 2018). Quite counter-intuitively, pancreatic cancer cells have been shown to speed up under high viscous conditions (Gonzalez-Molina et al. 2018).

Previous works by, Yizeng Li et. al., theoretically explored that water permeation can become an energy efficient mechanism for cells to migrate through high ECHR (Li et al. 2019; Li and Sun 2018).

The ECHR mediated by viscosity (which we will refer to as ECHR in this thesis) is rather a new phenomenon and in this thesis, we explore a method to estimate ECHR and a possible mechanism of motility of under high levels of ECHR which lead to cells speeding up.

1.2 Thesis overview

This thesis is constructed based on my research that I have performed over the past five years at Johns Hopkins University. It comprises two separate sections, 1) Estimation of the extracellular hydraulic resistance (ECHR) which forms *Chapter 2*, where we fundamentally explore both theoretically and experimentally the ECHR and from our rigorous insights, we come up with theoretical formulas to estimate ECHR, and 2) A possible mechanism of motility under viscosity mediated ECHR, which forms *Chapter 3*. We give experimental evidence of the theoretically concluded works of possible mechanism of motility under high viscosity and we ultimately link actin and water permeation mediated modes of cell migration.

The works of the section 1 have been published in the article:

Maity, Debonil, Yizeng Li, Yun Chen, and Sean X. Sun. 2019. “Response of Collagen Matrices under Pressure and Hydraulic Resistance in Hydrogels.” *Soft Matter* 15(12):2617–26

While the work of Section 2, is in preparation for publication:

Maity, Debonil, Kaustav Bera, Yizeng Li, Konstantinos Konstantopoulos and Sean X. Sun. 2020. “Extracellular Hydraulic Resistance Increases Cell Speed” (*in preparation*)

CHAPTER 2. ESTIMATION OF HYDRAULIC RESISTANCE

2.1 Introduction

Collagen is the primary extracellular matrix (ECM) protein and the most abundant protein in animal tissue. Collagen and collagen fibers in ECM play important roles in cell adhesion, migration, and differentiation (Beck et al. 2013; Doyle et al. 2015; Ferreira et al. 2007; Gerecht et al. 2007; Han et al. 2016; Kim et al. 2012; Nguyen-Ngoc et al. 2012; Provenzano, Inman, Eliceiri, Knittel, et al. 2008; Ray, Lee, et al. 2017; Ray, Slama, et al. 2017). Mechanical properties of ECM are important in tissue homeostasis, development, and progression of disease. Therefore, tensile and compressive behaviors of collagen ECM have been extensively studied, typically using external mechanical loading. Mechanical parameters associated with stiffness, viscoelasticity, and plasticity, have been quantified (Fratzl n.d.; Gautieri et al. 2012; Jansen et al. 2018; Licup et al. 2015; Mohammadi et al. 2015; Raub et al. 2007; Shen et al. 2011; Wisdom et al. 2018). From these studies, it is now clear that the matrix architecture is an important factor in determining ECM mechanics. For instance, it is recently reported that calcific aortic valve diseases are associated with layer-specific alterations in collagen architecture (Hutson et al. 2016). The collagen architecture is heterogeneous, and the matrix structure ranges from short-fibered collagen to increased fiber density and width. Different ECM architectures respond to external mechanical perturbations such as compression and shear differently (Ahmadzadeh et al. 2017; Riching et al. 2014), and some types of ECMs are more likely to expose the epithelium to damaging external mechanical forces (Casares et al. 2015). Indeed, Glioblastoma patients with more organized collagen architecture, characterized by a better degree of fiber alignment, have higher median survival compared to patients with less organized architecture (Pointer et al. 2017). Collagen architecture can be altered during the development of inflammatory disorders, aging, and fibrosis (Jeffery 2001; Liu et al. 2010). Such alterations can lead to even more damages to the tissue by making the epithelium more vulnerable (Casares et al. 2015). Since ECMs are hydrogels, the hydrodynamic properties of the collagen ECM could potentially influence cell mechanics and migration (Huber et al. 2018).

Recently, there is increasing recognition that cells may be sensitive to the hydraulic resistance that they experience (Li and Sun 2018; Prentice-Mott et al. 2013; Zanotelli et al. 2018). How the hydrodynamic variables of the matrix depend on collagen fiber architecture has not been explored. In this paper, we investigate the mechanical response of collagen matrices subjected to sudden changes in hydraulic pressure. We control the gelation temperature to vary collagen architecture (Doyle 2016). Furthermore, we modulate the stiffness of the collagen gel by chemical cross-linking (Sundararaghavan et al. 2008). To probe how different matrix architecture responds to mechanical loading, we develop a microfluidic device with a tubular matrix geometry, and apply external hydrostatic pressures (HPs) on the order of a few kPa and record the dynamic response of collagen hydrogels in the tubular configuration. We then use poroelastic theory to explain the observed response. Based on our estimates, we report biot-coefficient (Biot 1941) in the range of 0.94–0.98, a parameter which has been not studied previously while characterizing ECM mechanical properties (Gjorevski and Nelson 2012; Polacheck, Charest, and Kamm 2011). The developed microfluidic device is geometrically similar to the tubular epithelium commonly encountered in mammalian tissues. Therefore, MDCK II (Madin-Darby Canine kidney) epithelial cells are seeded on the inner surface of the collagen channel wall to form a confluent epithelium. We subjected the tubular epithelium to hydrostatic pressure changes and found that the tubular epithelium is much less deformable than the collagen matrix alone. To see how matrix architecture can influence matrix hydraulic properties, we studied hydraulic resistance experienced by a moving object in a 3D matrix based on the experimental parameters obtained above. We found that collagen permeability plays a dominant role in dictating hydraulic resistance experienced by the cell. Geometric confinement of the matrix can also significantly increase the hydraulic resistance due to increased restriction of pressure diffusion and fluid flow. We also found that along with the fluidic viscosity, the matrix shear stress can significant increase hydraulic resistance on a moving object within confined geometries. The scaling law for the hydraulic resistance remains the same for both a rigid and a viscoelastic object moving in the physiologically-relevant velocity regime. These results suggest that cells in 3D matrices *in vivo* can experience elevated hydraulic resistance, and fluid flow external to the cell is potentially another factor influencing mechanisms of cell motility.

2.2 Materials and Methods

A. Collagen Matrix Preparation

We used 7 mg/ml Rat tail type I collagen (Corning) for all experiments. We choose this concentration to make it as close as to physiologically-relevant values while avoiding collapse of the channel during fabrication. For the final concentration of 7 mg/ml, ~362 ml of the stock solution (9.66 mg/ml) was mixed with ~35 ml of 1N NaOH (Sigma, 795429) and ~103 ml of 10X DMEM (Sigma, D2429) (Nguyen-Ngoc et al. 2015). Then the collagen was allowed to gel for 1 hr at 37°C, or 24–36 hrs at 4°C. For matrix cross-linking, we used 0.01 mg/ml (0.04 mM) of genipin (Sigma, G4796), and incubated with an already gelled collagen substrate (which was previously gelled at 37°C) overnight at 37°C. Reflectance confocal images of the matrices are shown in Fig. 1A-C.

B. Microfluidic Device Fabrication

A polydimethylsiloxane (PDMS) block with a 1.1 mm × 2 mm × 1 cm rectangular hollow space is created using an aluminum mold, the dimensions of which are much larger than the collagen channel radius. Four holes are punched into the PDMS block after being removed from the aluminum mold and is plasma bonded onto a glass slide (Fig. 1D). A nitinol rod of 100 μm diameter is inserted into the rectangular channel. Poly-L-lysine coating (~1 hr at room temperature) is used to coat the inner surface of the PDMS channel to allow better adherence of collagen. Rat tail Type I collagen is used to fill the channel. Upon gelation, the interior holes are filled with Sylgard (Dow Corning) 164 (A: B = 10:1) and is allowed to cure for about 1 hr at room temperature. These act as support to the collagen block. The nitinol rod is then pulled out to create a channel of desired diameter. Sylgard 164 (A: B = 10:1) is also used to completely seal the ports located at the two ends of the collagen channel. When MDCK II cells are seeded in the channel, the nitinol rod diameter is increased to 150 μm.

C. Hydraulic Pressure Changes

Two 2.5mm diameter plastic tubes were connected at the outer ports, and were used to perform hydrostatic pressure perturbation. The tubes and the collagen channel were filled with PBS and the pressure was applied by raising the tube ends to height h (Fig. 1E).

D. Cell culture

We cultured cells in Dulbecco's modified Eagle's medium (DMEM) (Corning, 10013CV), 10% fetal bovine serum (FBS) (ATCC 30-2020) and 1% Pen/Strep (Sigma, P0781). The cells were a kind gift from Peter Searson Lab at the Johns Hopkins University. The cells were maintained in an incubator with 5% CO_2 at 37°C. Cells were then seeded into the tubular collagen channel and were allowed to line the inner surface of the channel. They were grown into a confluent epithelium after about a week of adherence.

E. Imaging and Image Analysis

We used Differential Interference Contrast (DIC) microscopy for acquiring images. Image acquisition was 14 frames per second. ImageJ and MATLAB were used to trace the diameters of the channel as a function of time. For imaging the collagen architecture, we used Confocal Reflectance Microscopy (CRM). CRM is a typical optical microscope modality used to visualize biopolymers such as collagen fibers.

2.3 Model description

We use poro-elastic theory to model the temporal response of the matrix during pressure perturbation (Cheng 2016). The governing equation for the solid phase, i.e., the collagen fibers, is

$$G\nabla^2\mathbf{u} + \frac{G}{1-2\nu}\nabla(\nabla\cdot\mathbf{u}) = \alpha\nabla p, [1]$$

where $\mathbf{u}$, G, ν, α are the displacement, shear modulus, Poisson's ratio, and the Biot-coefficient, respectively, of the solid phase. The symbol p is the hydrostatic pressure of

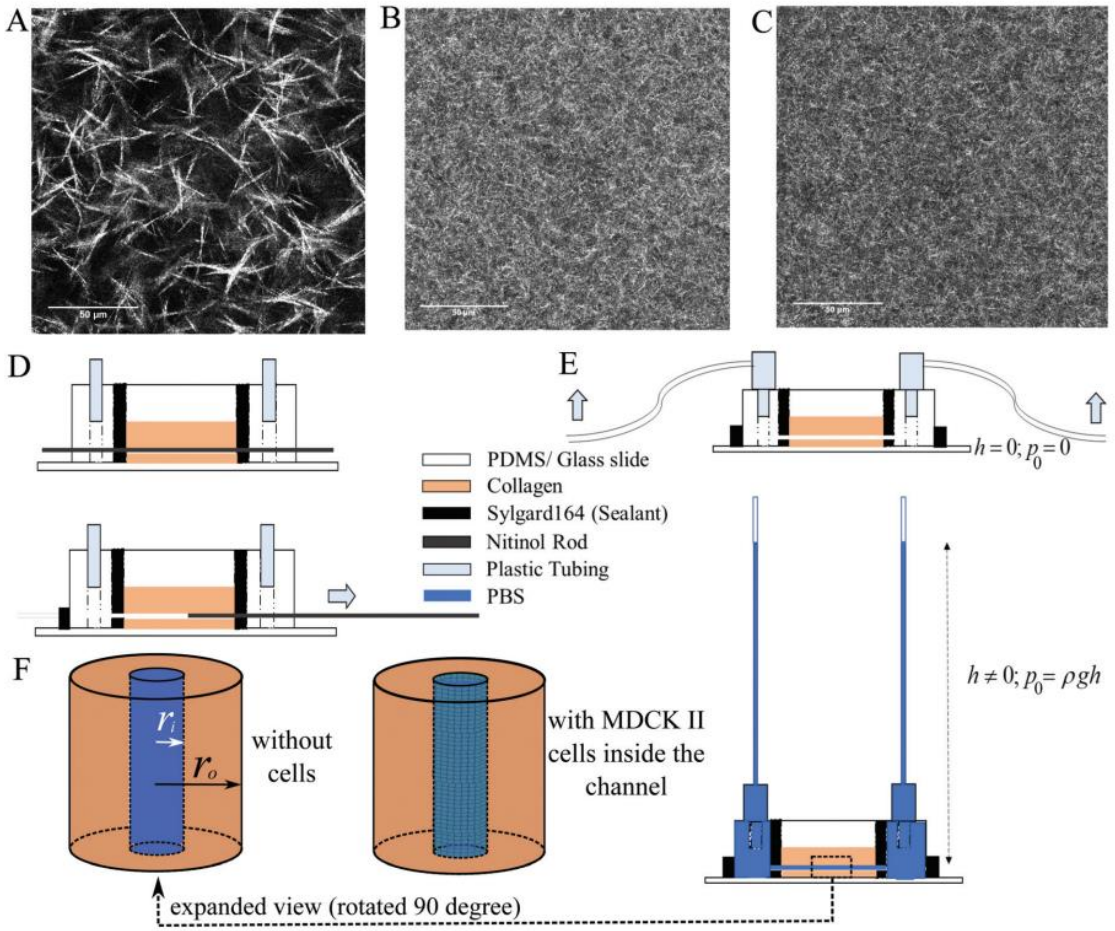

Fig. 1 (A–C) Collagen architecture for different gelation temperatures and levels of cross-linking, imaged using the reflectance mode. (A) 7 mg ml^{-1} gelled at 4 °C. (B) 7 mg ml^{-1} gelled at 37 °C. (C) 7 mg ml^{-1} gelled at 37 °C cross-linked with genipin. The collagen network gelled at 4 °C has thicker and longer fibers compared to the collagen gelled at 37 °C. The genipin cross-linking does not introduce significant differences in the fiber appearance. Scale bar = 50 μm. (D) Diagram describing the fabrication of the microfluidic device. After collagen is gelled in the microfluidic channel, a thin rod of diameter 100 μm or 150 μm is pulled from the device, leaving a channel of varying diameter. (E) Experimental setup for changing the hydraulic pressure. Tubes connected to the microchannel are raised and lowered to change the hydrostatic pressure in the channel. (F) Schematics of the channel (created by pulling the Nitinol Rod) filled with PBS with or without MDCK II cells lining in the inner face of the channel. The channel has an inner radius r_i = 50 μm and the boundary of the collagen is modeled by an outer radius r_o = 1050 μm. Drawn not to scale.

the fluid phase in the pores. The coupled consolidation equation of the fluid phase is

$$\frac{\partial p}{\partial t} - c\nabla^2 p = -\frac{\gamma}{(1+\nu)}\frac{\partial}{\partial t}\left(tr\boldsymbol{\sigma} + 4\eta p\right) \quad , [2]$$

where,

$$c = \frac{2\kappa\gamma G(1-\nu)}{\mu\alpha^2(1-2\nu)}, [3]$$

is the coefficient of consolidation, in which k is the permeability and μ is the dynamic viscosity of the fluid in the pores; and

$$\gamma = \frac{(\nu_u - \nu)}{(1-\nu_u)(1-2\nu)}, \quad \eta = \frac{\alpha(1-2\nu)}{2(1-\nu)}, [4]$$

where ν_u is the undrained Poisson's ratio and $\boldsymbol{\sigma}$ is the stress in the solid phase. Under plane strain, Eq. 2 becomes,

$$\frac{\partial p}{\partial t} - c\nabla^2 p = -\gamma(1-\nu)\frac{\partial}{\partial t}(tr\boldsymbol{\sigma} + 2\eta p), [5]$$

The constitutive relation is,

$$\sigma_{ii} = 2G\epsilon_{ii} + \frac{2G\nu}{1-2\nu} tr\boldsymbol{\epsilon} - \alpha p, [6]$$

and, $\boldsymbol{\epsilon} = \nabla \mathbf{u}$. The right hand sides of Eqs. 1 and 2 (or 5) show the coupling between the solid and the fluid phases. Eqs. 1 and 2 (or 5) are solved simultaneously by relevant boundary conditions of each problem. Since the Darcy's Law is implied in Eq. 2 (or 5), i.e.,

$$0 = -\nabla p - \frac{\mu}{\kappa}\mathbf{v}, [7]$$

the fluid velocity can then be post-calculated once p is solved. The full coupled system given by Eqs. 1 and 2 is solved by a finite element solver, COMSOL 5.1 (Debonil Maity et al. 2019; Paul et al. 2020; Poddar et al. 2016).

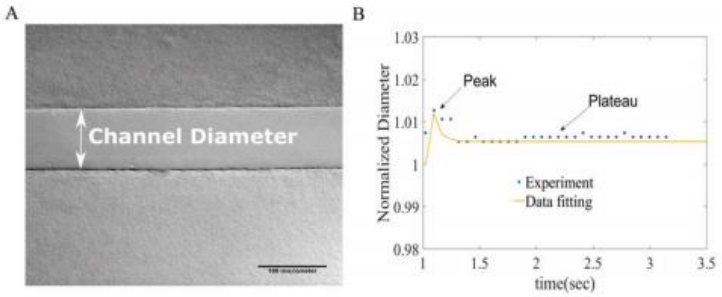

Fig. 2 Response of the collagen matrix to hydraulic pressure changes. (A) A DIC image of the collagen channel 100 μm in diameter. See Fig. 1F for a schematics where $2r_i$ = 100 μm. The diameter of the channel is monitored in time at 10 Hz resolution. (B) Data from pressure change experiment. The channel pressure is increased by five inches of PBS (~1.245 kPa) at t = 1 s, before which the normalized diameter is always 1. The peak (short time response) and plateau (long term response) are obtained from measuring the channel diameter as a function of time. The channel diameter recovers back to the original value after pressure release.

2.3.1 Temporal Response of the Matrix

The collagen channel in Fig. 2A can be treated as a hollow cylinder of inner radius r_i and outer radius r_0 (Fig. 1F). The principal stresses are σ_{rr} (radial) and $\sigma_{\theta\theta}$ (tangential). In cylindrical coordinates, the associated constitutive equations are,

$$\sigma_{rr} = 2G\epsilon_{rr} + \frac{2G\nu}{1-2\nu}(\epsilon_{rr}+\epsilon_{\theta\theta}) - \alpha p\,, [8]$$

$$\sigma_{\theta\theta} = 2G\epsilon_{\theta\theta} + \frac{2G\nu}{1-2\nu}(\epsilon_{rr}+\epsilon_{\theta\theta}) - \alpha p\,, [9]$$

where the strain components of the solid phase are $\epsilon_{rr} = \partial u_r/\partial r$ and $\epsilon_{\theta\theta} = u_r/r$. Under plane strain (Eq. 5), the fluid component is,

$$\frac{\partial p}{\partial t} - c\left(\frac{1}{r}\frac{\partial p}{\partial r} + \frac{\partial^2 p}{\partial r^2}\right) = -\gamma(1-\nu)\frac{\partial}{\partial t}(\sigma_{rr}+\sigma_{\theta\theta}+2\eta p)\,, [10]$$

At the inner radius $r = r_i$, the boundary conditions are .$\sigma_{rr}|_{r=r_i} = -p_0$ and $p|_{r=r_i} = p_0$. while at the outer radius $r = r_0$, the boundary conditions are $\partial p/\partial r|_{r=r_o} = 0$ and $u_r|_{r=r_o} = 0$. Here, p_0 is the applied hydrostatic pressure in the inner tube.

The parameters, $G, \alpha, \eta, c, \kappa, \nu, \nu_u$ are fitted to the channel diameter response observed in the experiments. μ is taken to be the value of water. Since the process of raising the hydraulic pressure in the tube is not infinitely fast, we assume a time-dependent increment in the pressure, $p_0(t) = p_0\left(1 - e^{-t/t_0}\right) / \left(1 + e^{-t/t_0}\right)$ where the constant $t_0 = 25$ s was chosen empirically to smoothly introduce a step-wise jump in pressure. The computed peak and plateau deformations are not sensitive to the precise form of this pressure change.

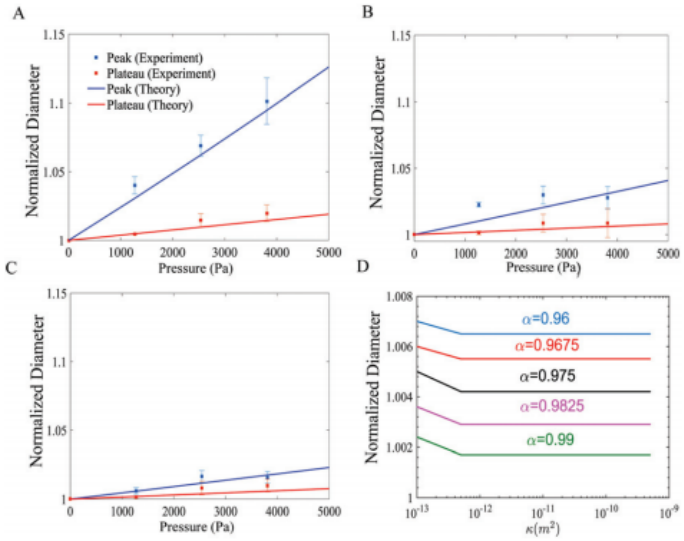

Fig. 3 Spatio-temporal response of collagen matrices of different architecture. (A) Peak and plateau deformations for 100 μm diameter channel with 7 mg ml^{-1} matrix gelled at 4 °C. Best fitting parameters obtained are: $\alpha = 0.97$, $G = 3.5$ kPa, $\nu = 0.2$, $\nu_u = 0.285$, $\kappa = 2.5 \times 10^{-11}$ m^2, $\mu \approx 10^{-3}$ Pa s. (B) Peak and plateau deformations for 100 μm channel with 7 mg ml^{-1} matrix gelled at 37 °C. Best fitting parameters obtained are: $\alpha = 0.98$, $G = 5$ kPa, $\nu = 0.2$, $\nu_u = 0.38$, $\kappa = 10^{-11}$ m^2. (C) Peak and plateau deformations for 100 μm channel with 7 mg ml^{-1} matrix gelled with 1% (w/v) genipin at 37 °C. Best fitting parameters obtained are: $\alpha = 0.98$, $G = 6$ kPa, $\nu = 0.2$, $\nu_u = 0.39$, $\kappa = 10^{-11}$ m^2. The difference between peak and plateau values is significantly larger for matrices gelled at 4 °C compared to 37 °C and genipin cross-linked collagen. (D) Predicted variations of channel plateau deformation as a function of matrix permeability, κ, and the Biot-coefficient, α. The rest of the parameters are the same as those in panel (A). The pressure change used was five inches of PBD (~1.245 kPa). We observe that beyond certain limit of permeability, the plateau is essentially independent of permeability. All error bars are standard errors.

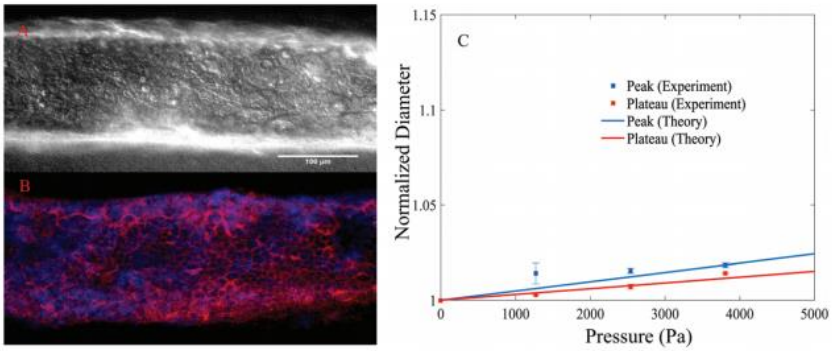

Fig. 4 Response of a model tubular epithelium in collagen gelled at 37 °C. (A) DIC image of a tubular epithelium showing a confluent layer of MDCK II cells in the collagen microchannel. (B) Confocal immunofluorescence images of the confluent MDCK II cells showing F-actin (phalloidin red) and nucleus (DAPI, blue). (C) Peak and plateau deformations of the tubular epithelium of MDCK II cells during hydraulic pressure change. Best fit parameters are: α = 0.94, G = 9 kPa, ν = 0.2, ν_u = 0.4, $\kappa = 5 \times 10^{-12}$ m^2. The channel deformation in the presence of epithelium is significantly smaller than that of the matrix without cells. This suggests that the epithelium resists pressure diffusion and fluid flow into the matrix. The error bars are standard errors.

2.3.2 Hydraulic Resistance Experienced by a Rigid Object Moving in Matrix

Cells moving in 3D matrices generally deform the solid phase of the matrix by exerting contractile forces (Bloom et al. 2008). Cells also remodel the matrix by actively digest existing collagen fibers while adding new fibers. To understand the hydraulic effect from the matrix to a moving cell, we first examine the hydraulic resistance experienced by a rigid sphere of constant velocity, v_0, in the matrix. To simplify the computation, we use cylindrical coordinate with axial symmetry, where the sphere moves along the axial, z, direction. The pore-pressure is governed by Eq. 2, where $tr\boldsymbol{\sigma} = \sigma_{rr} + \sigma_{\theta\theta} + \sigma_{zz}$. To solve the solid phase, we take time derivative of Eq. 11, i.e.,

$$G\nabla^2\mathbf{v} + \frac{G}{1-2\nu}\nabla(\nabla\cdot\mathbf{v}) = \alpha\frac{\partial}{\partial t}\nabla p, [11]$$

where $\mathbf{v} = \partial\mathbf{u}/\partial t$.

The computational domain is bounded by $r = R$ and $z = +/-l$. The boundary conditions are set as follows. At the surface of the sphere, non-slip condition for the solid phase is used, i.e., $v_z = v_0$ and $v_r = 0$. For the fluid phase, a non-penetration condition is used, i.e., $\nabla p \cdot \mathbf{n} = 0$, where $\boldsymbol{n}$ is the unit norm of a surface. We also require that the fluid at the surface of the sphere has the same axial velocity as the moving sphere, i.e., $\partial p/\partial z = -\mu v_0/\kappa$ by Darcy's law. So the non-penetration condition is rewritten as, $-z\mu v_0/\kappa + r\partial p/\partial r = 0$.

At r=R, $\boldsymbol{v}$=0 and $\partial p/\partial r = 0$. At z=+/-l, p=0 and $\boldsymbol{v}$=0. In the simulation, l=25 *mm* is fixed but R varies so that we can examine the effect of geometric confinement on the hydraulic resistance on the moving sphere. Unless otherwise specified or varied in each simulation, the default parameters used in this model

are: $k = 10^{-11}$ m^2, μ= 0.001 Pa.s, $\nu = 0.2$, $\nu_u = 0.39$, G = 6 kPa, α= 0:98, r_0 = 30 mm, v_0 = 1 nm/s, and $2R$ = 5 mm.

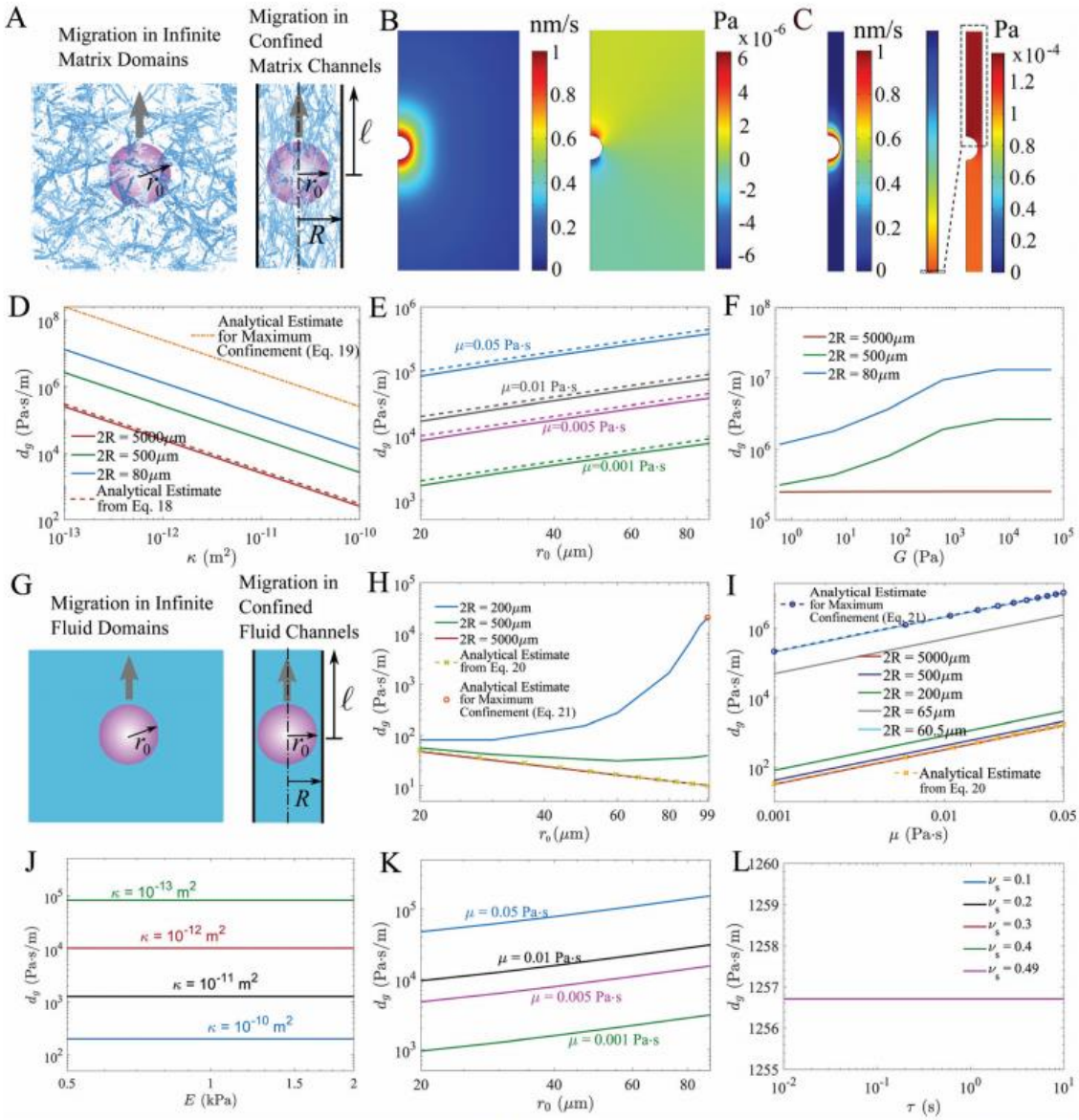

Fig. 5 Numerical simulations to estimate coefficient of hydraulic resistance, d_g. (A) Schematics of a spherical object moving upwards in axial, z, direction in a 3D poroelastic medium with different levels of confinement. (B and C) Left panels: The velocity of the solid phase from finite element (FE) simulations. Right panels: The fluid pressure field in the matrix pores from simulations. In (B) the radius of the channel is 2500 μm and in (C) the radius is 40 μm. Both pressure and velocities well decay to zero at the inlets and outlets of the channels. For better visualization, only part of the computational domain is shown (in C, the entire domain is shown). (D) Predicted coefficient of hydraulic resistance, d_g, as a function of κ for different channel confinement. Solid lines: predictions from FE simulations. Dashed line: analytical estimate of an infinite domain given by $d_g = \mu r_0/\kappa$ (eqn (18)). Dash-and-dotted line: analytical estimate of maximum confinement $d_g = \mu\ell/\kappa$. (E) Predicted coefficient of hydraulic resistance in the poroelastic medium, d_g, as a function of the radius of the spherical, r_0, for different fluid viscosities in the matrix, μ. Solid lines: predictions from FE simulation. Dashed lines: analytical estimate $d_g = \mu r_0/\kappa$ (eqn (18)). (F) Predicted coefficient of hydraulic resistance, d_g, as a function of the shear modulus of the solid, G, for different confinement dimensions. $\kappa = 10^{-13}$ m^2. (G) Schematics of a spherical object moving in a single phase (Stoke's flow) with different levels of confinement. (H) Predicted coefficient of hydraulic resistance, d_g, as a function of the radius of the spherical, r_0, for different channel confinement in Stoke's flow. Solid lines: predictions from FE simulations for Stoke's flow. Note d_g is significantly lower than in (E) for the same size object. (I) Predicted coefficient of hydraulic resistance, d_g, as a function of the fluid viscosity, μ, for different channel confinement. The solid lines are predictions from FE simulation. and the dashed lines with symbols are from analytical estimates. In (H) and (I), dashed lines with stars are analytical estimates for an infinite domain where $d_g = \mu/r_0$. Circles with or without dashed lines are analytical estimates $d_g = 8\mu\ell/R^2$, calculated from the position of the sphere to the end of the channel. (J–L) Prediction of d_g with a viscoelastic sphere from FE simulations. (J) Predicted d_g as a function of sphere elasticity, E, for different matrix permeability, κ. (K) Predicted d_g as a function of sphere radius, r_0, for different matrix viscosity, μ. (L) Predicted d_g as a function of sphere retardation time, τ, for different sphere Poisson's ratio, ν_s.

2.3.3 Hydraulic Resistance Experienced by a Viscoelastic Object Moving in Matrix

Here we extend our study to a viscoelastic object moving in 3D matrices and examine the scaling law of dg in this case. The geometry setup and the boundary conditions at $r = R$ and z =+/-l remains the same as the model described in Sec. 3.2. The interface between the collagen matrix and the object has non-slip condition modeled by the Fluid-Structure-Interaction module in COMSOL 5.1. Fluid movement in the collagen matrix is governed by the Darcy's Law with permeability k and dynamic viscosity μ; the viscoelastic object is described by the Kelvin-Voigt model with elasticity constant E, retardation time τ, and Poisson's ratio ν_s. Unless otherwise specified or varied in each simulation, the default parameters used in this model are: $k = 10^{-11}$ m^2, μ= 0.001 Pa.s, $\nu_s = 0.49$, G = 1 kPa, τ = 0.1 sec, r_0 = 30 mm, v_0 = 1 nm/s, and $2R$ = 5 mm.

2.4 Results and Discussion

2.4.1 Response of the Matrix to Hydraulic Pressure

To investigate how matrix architecture influence the matrix response to pressure changes, we vary the gelation temperatures and the presence of fiber cross-linking. It is known that increased gelation temperature and cross-linking leads to an increase in the matrix shear modulus (Doyle et al. 2015; Nguyen-Ngoc et al. 2015). Cross-linking does not cause any significant change in matrix pore size, or hydraulic permeability, as we qualitatively observe in Fig. 1A-C. To mimic physiological conditions, we adopted a tubular geometry, which is the typical structure of ductal epithelium in organs such as kidney, liver, or lung *in vivo*. We used a nitinol rod to create tubes of 100 μm in diameter as shown in Fig. 1D. This system allows us to employ sudden HP perturbation by raising the height h of the fluid in the connected channel (PBS/media), where the pressure is given

by $p_0 = \rho gh$, where g is the gravitational acceleration constant (Fig. 1E). We changed HP incrementally in fixed step size of 1.2 kPa, until reaching 3.6 kPa. A representative image of a typical collagen channel formed in our system is shown in Fig. 2A. We then measure the temporal mechanical response of the channel in terms of diameter changes by tracing the bound aries of the channel (Fig. 2A). The response typically shows a sudden peak in the collagen diameter upon the application of the HP, and a slower gradual relaxation to a final diameter that is different from the initial channel diameter before the application of HP change (Fig. 2B). When the HP is returned to zero, the channel diameter also recovers back to the original value, indicating that the channel is elastic (Gjorevski and Nelson 2012; Polacheck et al. 2011). To understand the observed response of collagen matrices to HP changes, we mathematically model the system using a linear poroelasticity theory, where the observed deformation peak is a function of shear modulus of the collagen, and the plateau is determined by both the permeability and shear modulus. Higher peak deformations correspond to lower matrix stiffness; lower plateau deformations correspond to higher hydraulic permeability (Fig. 3A-C). This type of response is explained by poroelasticity which couples fluid and solid phases of the matrix. Upon sudden hydrostatic loading, there is an initial elastic deformation of the channel which corresponds to the observed peak deformation. However, if the hydrostatic load is maintained, there is fluid influx which causes a dilation of the channel, which is the observed plateau (Fig. 2B). We can infer matrix poroelastic properties based on the magnitude of the peak, the magnitude of the plateau, and difference between the peak and the plateau.

The response of the matrix composed of 7 mg/ml of collagen gelled at 37^0C is shown in Fig. 3B. The shear modulus is found to be ~5 kPa. From Fig. 1A-C, we observe that the fibers at 37^0C gelation are shorter and denser compared to the 4^0C gelation. The permeability is found to be 10^{-11} m^2. For 4^0C gelation, as observed in (Raub et al. 2007), we observed that stiffness, as indicated by the shear modulus G, was significantly reduced to ~3.5 kPa, while permeability increased by 2.5 times.

The effect of crosslinking has been previously studied with various cross-linking agents such as glutaraldehyde and genipin (Miron-Mendoza, Seemann, and Grinnell 2010; Sundararaghavan et al. 2008). Cross-linking also increased the stiffness of the matrix by 1kPa, however, the permeability was not affected (Fig. 3B-C). From the poroelastic model, the magnitude of the plateau is determined by shear modulus, G, permeability, k, and biot-coefficient, α. The drop from peak to plateau indicates that the collagen is less deformed at steady-state due to water permeation into the collagen. Our theoretical work concludes that if α tends to 1, the difference between peak and plateau decreases (Fig. 3A, B).

2.4.2 Epithelial Layer Reduces Fluid Flow into the Collagen Matrix

We investigated the temporal response of the collagen matrix with epithelium lining the collagen channel. MDCK II cells were seeded on top of the fibronectin coated collagen channel walls and were allowed to grow to confluency (Fig. 4A, B). Once the epithelium was formed, we applied HP changes. We found that the channel is stiffer with an equivalent stiffness of ~9 kPa. Furthermore, the difference between peak and plateau was smaller than channels consisting of only collagen (Fig. 4C), which indicates that the effectively stiffer channel prevents large deformation. Since MDCK cells secrete fibronectin (Jiang, Chuang, and Tang 2000) and remodel the local interfacial matrix, the effect of the enhanced stiffness can be a combined effect of the MDCK epithelial sheet, the exogenous fibronectin, and the fibronectin secreted by MDCK cells and other ECM components. Moreover, we also observe that the permeability by fitting was reduced by an order of magnitude, suggesting that the epithelium is preventing pressure diffusion and fluid flow into the collagen matrix.

2.4.3 Hydraulic Resistance in the Collagen Matrix

The velocity and morphology of cells in a collagen matrix depend on the mechanical properties of the matrix. While the effects of matrix stiffness, density, alignment, and porosity on cell migration have been studied (Artym et al. 2015; Doyle et al. 2015; Fraley et al. 2010; Nam et al. 2016; Petrie and Yamada 2015; Provenzano, Inman, Eliceiri, Trier, et al. 2008; Ray, Slama, et al. 2017; Stein et al. 2011), the role of the hydraulic property of the matrix is less understood. Recent work suggested that the hydraulic resistance from the environment acting on cells can influence the mechanism of cell migration and cell speed (Li and Sun 2018; Prentice-Mott et al. 2013; Stroka et al. 2014; Zanotelli et al. 2018). The hydraulic resistance that the cell experience may be important in morphogenesis and cancer cell metastasis. A direct measurement of the magnitude of the hydraulic resistance in a matrix at cell scales is difficult. Therefore, based on estimated parameters obtained from experiments described above, we utilize numerical simulation to provide insights.

Schematics of a spherical object moving in 3D collagen matrix is shown in Fig. 5A. We examine the hydraulic resistance on objects in both infinite domains and confined channels. In all simulations the total length of the channel is $2l$ = 50 μm, which is large enough that all relevant fields decay to zero at z = +/-l. Steady-state is reached in a few hundred seconds; we obtain all results at t = 1,000 sec, where the sphere has moved 1 mm as we prescribe a constant sphere velocity v_0 = 1 nm/s. This velocity is chosen to be the same as typical cell migration velocities observed in matrices. Fig. 5B shows the computed velocity field of the solid phase (left panel) and the fluid pore pressure field (right panel) surrounding a moving sphere of radius r_0 = 30 μm in a channel of diameter $2R$ = 5000 μm. The solid phase has velocity v_0 on the surface of the sphere and the velocity decays in far field. The magnitude of the velocity is dominated by the velocity in the axial direction, which is about one order of magnitude higher than that in the radial direction. The fluid pressure, while decays to zero far away from the object, has non-zero values around the sphere.

When the channel diameter is reduced to 80 μm, the velocity
of the solid phase decays quickly to zero at $r = R$ (Fig. 5C, left panel). There is a column of fluid with non-zero pressure in front of the sphere (Fig. 5C, right panel). The size of the nonzero pressure region is larger for narrower channels because the fluid cannot easily pass around the sphere. The geometric confinement thus affects the hydraulic resistance experienced by the object moving in the matrix.

The coefficient of hydraulic resistance for a moving object, denoted as d_g, is defined as (Li and Sun 2018),

$$d_g = \frac{p_*}{v_0}, [12]$$

where p_* is the average fluid pressure acting on the front surface of the object. Simulation results show that dg varies inversely with the permeability of the matrix, k, (Fig. 5D). Moreover, we find that d_g is strongly affected by the confinement of the channel: it increases by about two orders of magnitude when the diameter of the channel decreases from 5,000 μm to 80 μm. A 5,000 μm channel is equivalent to the infinite domain limit as further increases in the channel width gives identical dg. These results indicate that a moving object experiences higher hydraulic resistance in confinement, even when the object does not completely occludes the confinement. This is also consistent with the idea that cell migration in 2D surfaces experiences less hydraulic resistance but when cells are confined in narrow channels, hydrodynamic effects from the environment is no longer negligible (Li and Sun 2018). This is significant because *in vivo*, cells migrating in 3D matrices are often also surrounded by other tissue such as the basement membrane, vessels, bones, and tendons. These objects provide confinement in the sense that they enforce vanishing fluid velocity on the object surface. This geometric confinement changes the pressure field in the matrix and increases the apparent hydraulic resistance by orders of magnitude.

The coefficient of hydraulic resistance, *dg*, also increases linearly with the radius of the sphere and the viscosity of the fluid in the media (Fig. 5E). The influence of the shear modules of the matrix, *G*, however, depends on the confinement (Fig. 5F). In infinite domains *dg* does not vary with *G* while in confined domains dg increases with increasing *G* and saturates at about *G* = 1 kPa. The narrower the channel, the larger the influence of *G* has on *dg*. This result suggests that the stiffness of the collagen matrix affects cell migration not only through adhesion formation but also potentially through hydraulic resistance. This influence is present in confined channels and also in tissue spaces as large as 500 μm in the cross-section. We shall mention that in the simulation we have allowed the collagen matrix to deform up to 1 μm when the object moves. The magnitude of the deformation may vary when the matrix is rapidly dissolved by cells during cell migration, which we will discuss in the next section. When, however, the matrix does deform by a small amount, our simulation implicates non-trivial effect of the matrix stiffness on the hydraulic properties. Future experimental work will uncover the dual role of matrix stiffness on cell migration in 3D collagen matrix.

2.4.4 Scaling Laws of *dg* in Collagen Matrix

Numerical results show that d_g depends on the fluid properties within the matrix as well as the geometry of the moving object and the domain. To understand this further, we derive an analytical approximation of d_g to obtain a scaling law of the dependence of d_g on the matrix properties. During *in vivo* cell migration, cells secrete matrix metalloproteinases (MMPs) (Baker and Chen 2012) which dissolve the collagen structure of the matrix. For this reason, the matrix does not deform continuously as cells migrate further. In the limit that MMPs fully dissolve the matrix, no strain or stress is developed within the matrix solid phase. In this case, we can simplify the full system by neglecting Eq. 1 and using an uncoupled version of Eq. 2, i.e.,

$$\frac{\partial p}{\partial t} - c\nabla^2 p = 0\,, [13]$$

We first derive the scaling law of dg for a spherical object moving in an infinite domain compared to the size of the object. The front of the spherical object moves at velocity v_0, which acts as a continuous pressure source in space and time that pushes the fluid in the collagen matrix. To simplify the matter, we may focus on each instantaneous moment where the pressure source is spatially fixed. In this case, the pressure source at the front of the object can be considered as a Dirac delta function in time with an amplitude p_* that serves as a boundary condition for the pore pressure in the matrix. In this case, the pressure field radiating from the object is spherically symmetric. The consolidation equation is best solved in the frequency domain with a time harmonic form, $p = \tilde{p}\exp(i\omega t)$, where the tilde denotes a quantity in the frequency domain. Eq. 13 then becomes

$$\frac{\partial^2}{\partial r^2}(r\tilde{p}) - \frac{i\omega}{c}(r\tilde{p}) = 0\,, [14]$$

An infinite domain implies that there is no wave reflection. Therefore, the solution to Eq. 14 is

$$\tilde{p} = \tilde{p}_* \frac{r_0}{r} e^{\sqrt{\frac{i\omega}{c}}(r_0 - r)} = \tilde{p}_* \frac{r_0}{r} e^{\sqrt{\frac{\omega}{2c}}(1+i)(r_0 - r)}\,, [15]$$

where p_* is the pore pressure on the sphere associated with frequency w. The pressures $\tilde{p}_*$ and p_* have the same value in number since the pressure source is a delta function in time. From the decay rate in Eq. 15, the length scale of the pressure wave propagation is $L_p = \sqrt{2c/\omega}$, which decreases with increasing frequency. In the spherical coordinate the fluid velocity in the radial direction, v_r, can be solved from the Darcy's Law (Eq. 7) as $v_r = -(\kappa/\mu)\partial p/\partial r$. The boundary condition of v_r is

$$v_r\big|_{r=r_0} = -\frac{\kappa}{\mu}\frac{\partial p}{\partial r}\big|_{r=r_0} = v_0\,, [16]$$

which can also be written in the frequency domain. The combination of Eqs. 15 and 16 gives the coefficient of hydraulic resistance in the frequency domain

$$\tilde{d}_g = \frac{\mu}{\kappa}\left[\frac{1}{r_0} + \sqrt{\frac{\omega}{2c}}(1+i)\right]^{-1}, [17]$$

The dominant ones are those of low frequencies. Indeed, as seen in Eq. 15, components of high frequencies are unable to propagate through long distance. On the first order of approximation, the coefficient of hydraulic resistance in collagen matrix is

$$d_g \approx \frac{\mu r_0}{\kappa}, [18]$$

which provides a clear scaling law for d_g in infinite domains: d_g varies linearly with the viscosity of the fluid in the pores, μ, and the radius of the spherical object, r_0, and varies inversely with the permeability of the collagen matrix, k. Using Eq. 18 is equivalent to assuming that the fluid in the pore is incompressible such that the consolidation equation (Eq. 13) is reduced to $\nabla^2 p = 0$. This analytical approximation (Eq. 18) matches well with the numerical simulation in approximately infinite domains (Fig. 5D, E), although some negligible over-estimation is found, which can also be seen from Eq. 17. The agreement of the two solutions also indicates that in infinite domains the mechanics of the solid phase does not play a significant role in setting up d_g, as shown in Fig. 5F. We can compare to the case that the moving object is maximally confined where $R = r_0$. Here in order for the object to move, it must push the complete column of fluid in front of it. Using Darcy's law, the pressure gradient can be solved by $v_0 = -(\kappa/\mu)\partial p/\partial r$. Hence, for a channel of length l at the front of the object, the coefficient of hydraulic resistance is

$$d_g = \frac{\mu \ell}{\kappa}, [19]$$

which is about an order of magnitude higher than that from the 80 μm confinement within the poroelastic medium. This solution represents the maximal limit for d_g in confinement. It is also useful to compare hydraulic resistance of a moving object in pure fluid, the so called Stoke's flow limit (Fig. 5G). A moving sphere with radius r_0 and velocity v_0 in an infinite fluid medium has a total drag force $6\pi\mu r_0 v_0$, in which one-third comes from the pressure drag (Durst n.d.). By considering the average pressure acting on the front surface of the sphere, the corresponding coefficient of hydraulic resistance is

$$d_g = \frac{\mu}{r_0}, [20]$$

which is inversely propositional to r_0, as opposed to the linear dependence on r_0 in porous media (Eq. 18). The r_0^{-1} dependence in Stokes flow is confirmed in simulations for a domain with $2R$ = 5000 μm (Fig. 5H). Unlike the porous medium, the dependence of d_g on r_0 in Stokes flow varies with the confinement. When channels become narrower, d_g starts to increase with increasing r_0. In the limit that the radius of the sphere is close to the radius of the channel, i.e., r_0 approximately equal to R, the coefficient of hydraulic resistance of the maximum confinement case can be solved:

$$d_g = \frac{8\mu\ell}{R^2} [21]$$

Indeed, when the r_0 approaches R, the d_g from simulations matches Eq. 21 (Fig. 5H, I). Finally, in Stokes flow dg also increases linearly with the viscosity of the fluid (Fig. 5I) regardless of the confinement (Eq. 20 and 21). Overall, d_g generally increases when the sphere migrates in a more confined geometry (Fig. 5H, I). This is because a sphere in an infinite domain only generates fluid flow around it, but when a sphere is placed in a channel of the same radius as the sphere, it displaces the entire column of fluid in the channel when moving.

The presence of the matrix also can increase the hydraulic resistance by several orders of magnitude. Therefore, the hydraulic resistance is a function of matrix properties as well as the microenvironment geometry.

The above simulations show the scaling law of dg for a rigid sphere moving either in a poroelastic medium or in Stokes flow. We next examine the scaling low of dg for a viscoelastic sphere moving in a medium governed by Darcy's Law. For an object moving v_0 = 1 nm/s, d_g does not depend on the elasticity of the object (Fig. 5J). d_g still scales inversely with the medium permeability (Fig. 5J). It also scales linearly with the radius of the object and the viscosity of the medium (Fig. 5K). However, d_g does not depend on the retardation time nor the Poisson's ratio of the sphere object (Fig. 5L). Collectively, our results suggest a general scaling law of d_g on k and r_0 for an object moving at physiologically relevant velocity in a porous medium.

2.5 Conclusions

Porous hydrogels such as collagen matrices are important microenvironments where cells can proliferate and migrate. The physical properties of these hydrogels can influence fundamental cell functions. Here we developed a microfluidic method of measuring response of the matrix against changes in hydraulic pressure. Our device is specially suited for studying the tumor microenvironment (Wong and Searson 2014) which is stiffer than normal tissue matrices and promotes cell migration (Gkretsi and Stylianopoulos 2018). Using a poroelastic model, our approach is able to obtain poroelastic parameters such as the permeability, the Biot coefficient, and the shear modulus in a single experiment. This is in contrast with methods that can measure the permeability alone (Gjorevski and Nelson 2012; Polacheck et al. 2011). The method is able to discern differences between matrices of different fibrous architecture. Within the same microfabricated matrix, we also examined fluidic permeability of a confluent epithelial tubule and found that the epithelial cells can resist pressure changes. In addition to matrix mechanical properties, the matrix hydraulic resistance may also influence cell migration.

Here we explore using numerical simulations how the hydraulic resistance in the matrix depends on matrix permeability as well as matrix stiffness. The results show, unsurprisingly, that a moving object experiences higher hydraulic resistance in confined matrices. What is perhaps surprising is the degree of increase: d_g experienced by the cell can be 10^3 times higher in a confined matrix when compared to the d_g in an infinite matrix. This level of increase holds for all values of permeability (Fig. 5D). The range of permeability we have studied, from 10^{-13} m^2 to 10^{-10} m^2, are the numbers that are typically reported in literature for collagen of concentrations varying from ~2 mg/ml to ~10 mg/ml (Antoine, Vlachos, and Rylander 2015; Gjorevski and Nelson 2012; Jansen et al. 2018; Mason et al. 2013; Polacheck et al. 2011). The increase in d_g is even larger (up to 10^7 time higher depending on the matrix permeability) between a cell in a confined matrix and cells in 2D fluidic culture environment (Fig. 5D, H). In addition, increasing matrix shear modulus, which describes a stiffer matrix, can also increase the hydraulic resistance by several fold for small geometric confinement. These findings suggest that matrix mechanical properties may have multiple effects on cell behavior in realistic biological settings.

CHAPTER 3. A MECHANISM OF CELL MOTILITY UNDER HIGH HYDRAULIC RESISTANCE

3.1 Introduction

Cells *in vivo* experience a diverse microenvironment that can dramatically influence major biological processes such as cell migration, tissue homeostasis, repair and disease (de Lucas, Pérez, and Gálvez 2017; Trepat, Chen, and Jacobson 2012; Vicente-Manzanares 2005). One such physical factor is the extracellular hydraulic resistance (ECHR), which is a measure of how freely fluids can flow external to the cell. ECHR is known to affect both the direction and speed of cell migration (Zhao et al. 2019) and depends on the geometry of the microenvironment immediately surrounding the cell. For instance, in confining microchannels, ECHR is significantly elevated, and is proportional to the length of the microchannel and inversely proportional to the channel cross-sectional area (D. Maity et al. 2019). In the collagen-rich extracellular scaffold, ECHR experienced by migrating cells can be several orders of magnitude higher than in 2D cell culture (D. Maity et al. 2019). Another equally important factor that influences hydraulic resistance is the viscosity of the fluid surrounding the cell(D. Maity et al. 2019). Indeed, ECHR is directly proportional to fluid viscosity. *In vivo*, fluids containing significant concentrations of macromolecules are known to have elevated viscosity: Synovial fluid has been demonstrated to have viscosity of about 0.9Pa.s (Roselli and Diller 2011). Human gastric mucus has a viscosity of about 6 Pa.s (Roselli and Diller 2011). Airway mucus shows viscosities between 1-2.3 Pa.s (Roselli and Diller 2011). Human blood has been known to demonstrate viscosity of about 0.005 Pa.s(Furukawa et al. 2016). The presence of glucose further enhances the viscosity of the blood(Çinar 2001). In comparison, water viscosity is significantly lower, ~0.001Pa.s. Thus, cells are likely to encounter high viscosity fluids and various physical confinement/obstacles while navigating in tissues *in vivo*. During cancer metastasis, cancer cells must migrate through the primary tumor site, stroma, endothelium, vascular system, and the tissue at the secondary tumor location (Wirtz, Konstantopoulos, and Searson 2011). Along these steps, cancer cells are likely to encounter both physical confinement, ECM of varying densities, and fluids with high viscosity.

Thus, the hydraulic resistance experienced by cancer cells can be orders of magnitude higher than what is experienced in cell culture in 2D.

Elevated ECHR is equivalent to an elevated hydraulic pressure surrounding the cell during cell migration. Since in order for the cell to move, the surrounding fluid must also move, a pressure gradient is developed around the cell. Theoretically, this pressure gradient is directly proportional to the ECHR(D. Maity et al. 2019). Recent data have shown that tissue cells are extraordinarily sensitive to hydraulic pressures (Zhao et al. 2019). A pressure rise of a few pascals can lead to dramatic cell responses (Zhao et al. 2019). Therefore, cell response to ECHR is also related to cell pressure sensing. Here, we explore the effects of elevated ECHR by examining 2D cell migration in high viscosity fluids. We show that, contrary to intuition which predicts that motions of objects slow down in high viscosity media due to increased fluid dynamic drag, animal cells such as MDA-MB-231 migrate faster in high viscosity fluids. The molecular mechanisms that give rise to this speed increase is explored in this paper.

Cell migration is classically understood as the result of actin polymerization at the cell leading edge, cytoskeletal contraction mediated by myosin-II, and assembly or disassembly of integrin dependent adhesions (Craig et al. 2015; Gardel et al. 2010; Pollard and Borisy 2003; Shao, Levine, and Rappel 2012). The influence of factors such as the mechanical properties of the 3D matrix, focal adhesion proteins, lamina and LINC complexes (Doyle et al. 2015; Even-Ram and Yamada 2005; Petrie and Yamada 2012; Wu, Gilkes, and Wirtz 2018; Yamada and Sixt 2019) on actin-driven cell migration has been extensively studied in 2D culture. In addition to the actin mechanism, Stroka *et.al.*, showed that water permeation driven by ionic gradients generated by the cell can also drive migration in narrow confining channels (Stroka et al. 2014). In this osmotic engine model (OEM), it was shown that Na^+/H^+ ion exchanger is involved in water-driven cell migration. NHE1 and several other ion-channels such as sodium-potassium-chloride co-transporter 1 (NKCC1) and sodium-potassium (NaK) pump (Chen et al. 2014; Cong et al. 2015; Ma et al. 2019; Mathieu et al. 2009; Repke 1988; Shiozaki 2014; Simpson et al. 2009; Zhou et al. 2017) have also been previously implicated in cancer, and maybe involved in metastasis and OEM.

Li *et.al.*, using a two-phase model of the cytoplasm, has theoretically explored the transition from actin-driven to water-driven mechanism of cell migration (Li and Sun 2018). The model predicted that with no change in molecular elements driving motility, cells can speed up under high hydraulic resistance.

Here we present experimental evidence of combined actions of actin- and water-driven cell migration in high extracellular fluid viscosity environments. We demonstrate the critical role of ion-channels/ ion-pumps in dictating motility in high viscosity fluids. Furthermore, we show that inhibition of vesicle trafficking, which impedes ion-channel trafficking and re-distribution, also inhibits cell migration in high viscosity environments. Results suggest a dual role of F-actin for motility in high viscosity conditions: it is not only involving in extending the cell leading edge, it is also involved in directing vesicular transport and positioning of ion channels that facilitate water intake. Taken together, we find that water and F-actin both contribute to the final cell speed observed in high viscosity environments.

3.2 Materials and Methods

3.2.1 Cell culture

MDA-MB 231, HT1080, 3T3 and Sum 159 cells were kind gifts from the lab of Prof. Konstantinos Konstantopoulos. All cells were cultured in DMEM (ThermoFisher 11995065), 10% (by volume) FBS (Sigma-Aldrich) and 1% (by volume) penicillin/ streptomycin (Gibco) at 37^0C and 5%CO_2.

3.2.2 Immunostaining

For immunostaining we treated the cells with pertinent drugs or no drugs. After treatment times, we fixed them using Paraformaldehyde Solution (4% in PBS, ThermoScientific J19943K2) for 15min at Room temperature (RT). After fixation, cells were washed with PBS, three times for a duration of 5min each. They were then permeabilized using 0.5% (by volume) Triton-X (Sigma Aldrich X100) in PBS for 10min at RT. After permeabilization, the cells were washed with PBS in three steps.

Then the cells were subjected to blocking agent 2% (by volume) Bovine Serum Albumin (BSA) (Sigma Aldrich A7906) in PBS for 30min at RT. Then we proceeded with the steps of incubation with primary/ secondary antibodies in 1% BSA solution for a period of 1hr at RT each. The incubation with primary and/or secondary antibodies were followed by the three step washing with PBS. For F-Actin staining, we used Alexa Fluor™ 647 Phalloidin (ThermoFisher A22287) in 1:100 volumetric ratio in 1% BSA. For Vinculin staining, we used Vinculin Monoclonal Antibody (7F9), Alexa Fluor 488 (ThermoFisher 53-9777-82) in 1:25 volumetric ratio in 1% BSA. For staining of pMLC, we used 1:2000 Primary: Anti-Myosin light chain (phospho S20) antibody (Abcam ab2480) and 1:250 Secondary: Goat Anti-Rabbit IgG H&L (Alexa Fluor® 488) (Abcam ab150077) volumetric ratio in 1% BSA. For NKCC1 staining we used 1:100 Primary NKCC1 (D13A9) Rabbit mAb (Cell Signalling Technology 8351) and 1:100 Secondary Alexa Fluor® 488 AffiniPure Goat Anti-Rabbit IgG (H+L) (Jackson Immuno 111-545-003). For NHE1 staining we used 1:100 Primary (B-12) (Santa Cruz sc-515950) and 1:100 Secondary Goat anti-Mouse IgG (H+L) Cross-Adsorbed Secondary Antibody, Alexa Fluor 488 (ThermoFisher A-11001). For NaK staining we used 1:100 Primary Anti-Na+/K+ ATPase α-1 Antibody, clone (Sigma Aldrich 05-369) and 1:100 Secondary Anti-mouse IgG (H+L) (Cell Signalling Technology 4409S). All are in volumetric ratio in 1%BSA.

3.2.3 Cell Speed measurements, fluorescence analysis

Cell speeds were taken using DIC (5hrs, 10min intervals) and fluorescence were imaged using Epifluorescence in a Zeiss LSM 800 system. For cell speeds, a 10X air objective was used. For immunostaining images, 40X objective was used. Cell speeds and fluorescent images were hand traced. For the analysis of immunostaining the local background noise was subtracted from the mean intensity of the demonstrated by the cells. For total distance, displacement and persistence calculations, the location of the cells obtained from 10X DIC imaging were utilized. For focal adhesion images, we used 63X objective and confocal in a Zeiss LSM 800 system. For focal adhesion area to cell area ratio, we used image-thresholding to segregate focal adhesions. Then total area of focal adhesions was obtained calculating the number of non-zero pixels. Cell area was calculated by hand tracing. MATLAB and ImageJ were used for all image analysis.

3.2.4 Retrograde flow measurements

For retrograde flow measurements, we transiently transfected the cells using pEGFP-C1 F-tractin-EGFP which is a gift from Dyche Mullins (Addgene plasmid # 58473). After ~20hrs, the cells were incubated with fresh control media, or the high viscosity media and then imaged using 63X Confocal (3min, 3sec intervals). We used particle image velocimetry (PIVLab) for our analysis.

3.2.5 Calcium imaging

For Calcium imaging, we transiently transfected the cells with pGP-CMV-GCaMP6m which is a gift from Douglas Kim (Addgene plasmid # 40754). After ~20hrs, the cells were incubated with fresh control media, or the high viscosity media and then imaged using 40X Epifluorescence (5min, 1sec intervals). After Fast Fourier Transform of the Calcium signals, power versus frequency were plotted normalized relative to the maximum power (global maxima of the power versus frequency).Then the spectrum was divided into several bins, namely, Bin 1: 0-100mHz, Bin 2: 100-200mHz, Bin 3: 200-300mHz, Bin 4: 300-400mHz and Bin 5: 400-500mHz. For mean relative peak power, the average of the powers of the peaks (points of local maxima) in a specific bin was taken, and for maximum relative peak power, the maximum power in a bin was taken and it was divided by the total number of peaks in that specific bin.

3.2.6 Traction force microscopy

For 2D substrate preparation, we used the protocol as described in a previous article (Sao et al. 2019). After the substrate preparation, it was coated with 20ug/ml of rat tail type I collagen (Corning) and incubated in 37^0C for 1hr. After gently taking out the collagen solution, we seeded the cells over a duration of ~20hrs to allow them enough time to adhere and spread out. For performing traction force experiments, we used a 40X objective, and used trypsinization to make the cells detach. We imaged samples before trypsinization and ~30min after trypsinization. The bead displacements were recorded and the ensuing images were analyzed as described in a previous article (Sao et al. 2019).

3.2.7 Viscosity media preparations

For preparation of hydroxyl-propyl-methylcellulose, we used 0.25%, 0.5% and 1% (weight/ volume) of Methocel J75MS (Dow), in cell culture media. For 1% (weight/ volume in cell culture media) Low viscosity and Media viscosity sodium alginate we used Alginic acid sodium salt from brown algae (Sigma Aldrich Low- A1112 and Medium A2033 viscosity respectively). For 5% (weight/ volume in cell culture media) Dextran solution, we used Dextran from Leuconostoc spp. (Sigma Aldrich 31390). Immediately after mixing the solutes, the solution was subjected to a constant rotation at 10 rpm at RT over a period of ~1-2days in order to achieve a uniform mixture. The viscosity values were measured using a rheometer.

3.2.8 Inhibition experiments

We used Latrunculin A (Sigma-Aldrich), 5-(N-Ethyl-N-isopropyl) amiloride (EIPA, Sigma Aldrich), Ouabain (Sigma-Aldrich), Bumetanide (Ro 10-6338, Santa Cruz Biotechnology), Rab7 inhibitior CID 1067700 (Sigma-Aldrich), MyoVin-1 (Sigma-Aldrich), BAPTA-AM (Sigma-Aldrich), FTY720 (Tocris Biosciences), Calpain inhibitor I (Millipore Sigma) in dimethylsulfoxide and Gadolinium (III) Chloride (Sigma-Aldrich) in water. For all inhibition experiments, cells were incubated in cell culture media with drugs for a duration of 1hr (except Ouabain ~2hrs) and then high viscosity media was added. Cells were then imaged over a span of 5hrs for speed measurements or were incubated over a span of ~4hrs for immunostaining.

3.2.9 Collagen gel preparation and 3D cell speed acquisition

For collagen gelation, we used the protocol described in a previous publication(Fraley et al. 2010). Cells in 1:1 (volume/volume) ratio of cell culture media and reconstitution buffer were mixed with the appropriate volume of rat-tail type I collagen (Corning) to obtain a final collagen I concentration of 1 mg/ml. A pertinent calculated amount of 1 M NaOH was quickly added. Cells were allowed to spread out over a duration of ~6-8hrs and then pharmacological inhibition experiments were performed. X-Y displacement of the cells were acquired using 20X DIC (7hrs, 10min intervals).

3.2.10 Cloning, lentivirus preparation and transduction

To generate MDA-MB-231 cells with stable knock down of NKCC1, pLKO.1 puro (plasmid no. 8453; Addgene, Cambride, MA; a gift from B.Weinberg) backbone was used. Non-specific scramble sequence (5'-GCACTACCAGAGCTAACTCAGATAGTACT-3'), shNKCC1 sequence-1 (5'-ACCAAATTTCATCCATATATC-3'), shNKCC1 sequence-2 (5'-GCCACTCTTTCTTCAGCATTA-3') and shNKCC1 sequence-3 (5'-GCCACTCTTTCTTCAGCATTA-3') were subcloned into the backbone. For producing lentivirus 293T/17 cells were co-transfected with psPAX2, pMD2.G and the lentiviral plasmid. 48h after transfection lentivirus was harvested and concentrated using centrifugation. Wild type MDA-MB231 cells at 60-80% confluency were incubated for 24 h with 100X virus suspension and 8 µg/ml of Polybrene Transfection Reagent (Millipore Sigma). To maintain stable knock down, virus transduced cells were grown in media containing 0.5 µg/ml Puromycin (Gibco).

3.3 Results

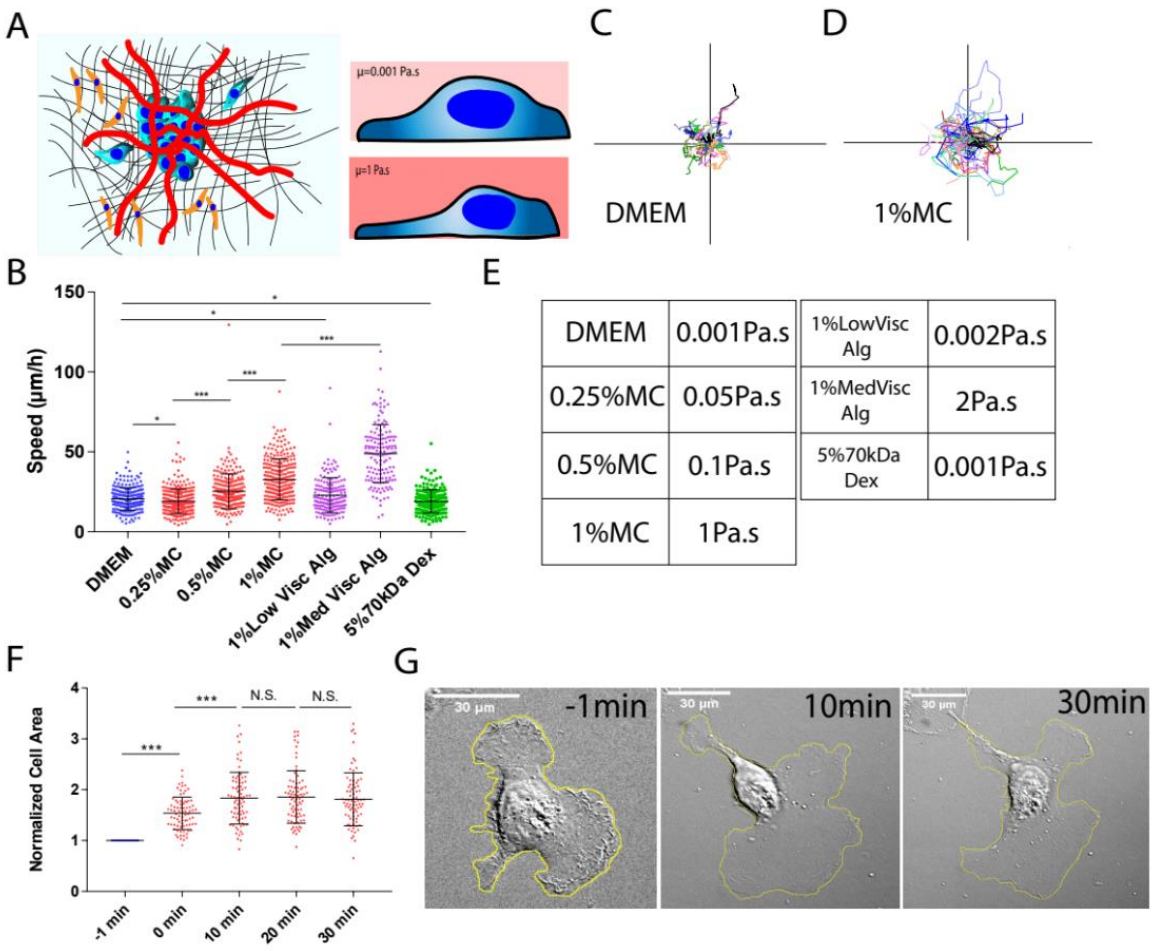

Figure 1- Cell speed is a function of cell media viscosity (A) Graphical representation of the tumor microenvironment and cells in low and high viscosity media (B) Cell Speed is dependent is purely dependent on viscosity as represented by speeds of MDA-MB 231 cells in DMEM (N=253), 0.25%MC (N=295), 0.5%MC (N=250), 1%MC (N=278) and not the property of the thickening agent added as represented by speeds in 1% low (N=167) and 1% medium viscosity (N=148) alginate or the number of solutes added to system as represented by speed in 5% 70kDa Dextran (N=199) (C) , (D) Representation of typical tracks of MDA-MB 231 cells in DMEM and 1%MC respectively (E) Viscosities of solutes used (F), (G) Cell Area change with addition of high viscosity medium (N=79 cells) (H) Pictorial representation of the definition of persistence. *p<0.05, **p<0.005 and ***p<0.0005 across all plots.

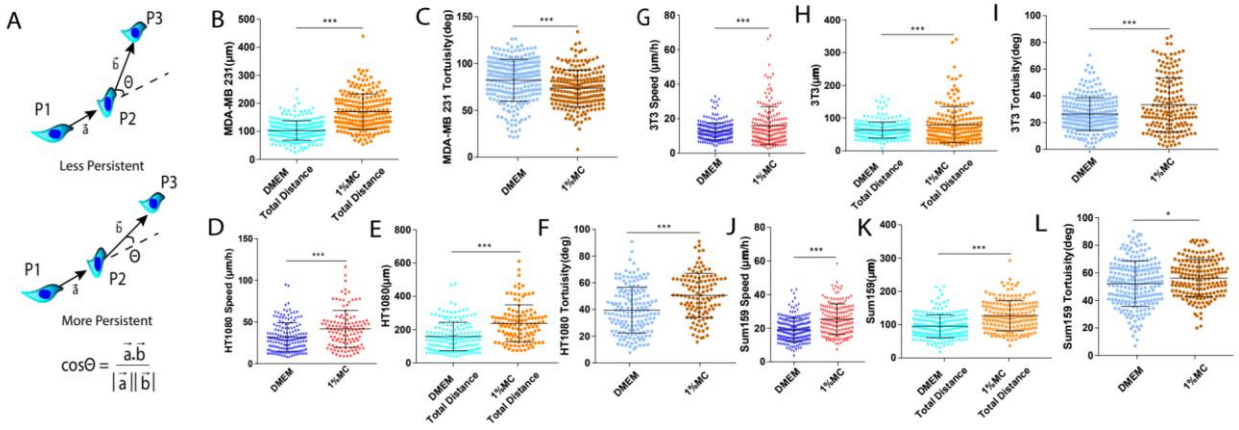

Figure S1- Cell speed and total distance travelled increase with viscosity for different cell lines and investigation of tortuisity with as a function of viscosity (A), (B) Total distance travelled and tortuisity of MDA-MB 231 in DMEM (N=253) and 1%MC (N=213) respectively (C), (D), (E) Speed, total distance travelled and tortuisity of HT1080 cells in DMEM (N=165) and 1%MC (N=119) (F), (G), (H) Speed, total distance travelled and tortuisity of 3T3 cells in DMEM (N=247) and 1%MC (N=176) (I), (J), (K) Speed, total distance travelled and tortuisity of Sum159 cells in DMEM (N=221) and 1%MC (N=176).

3.3.1 Increased media viscosity increases cell speed while osmolarity increase does not

The microenvironment *in vivo* can dramatically increase the extracellular hydraulic resistance (ECHR). The ECHR is also directly proportional to the viscosity of the extra-cellular fluid. To investigate the effect of ECHR on migrating single cells, we examined MDA-MB-231 cells in 2D culture in media with thickening agents such as hydroxy-propyl-methylcellulose (MC) and low/medium viscosity sodium alginate. With increasing % weight of MC (viscosities ranged from 0.05 Pa.s to 1Pa.s, compared to control media, where the viscosity was 0.001Pa.s. All viscosities were measured using a rheometer), we observed a gradual cell speed increase (Fig 1B). The same trend was observed with low (0.002 Pa.s) and intermediate (2 Pa.s) viscosity media with sodium alginate, implying that the speed increase does not depend on the chemical composition of the thickening agent. The effective viscosities will remain roughly constant in the domain of the cell speed (Maity, Bandopadhyay, and Chakraborty 2016; Paul et al. 2020).

To check that the observed speed increase is not due to media osmolarity increase, we also used media with 5% 70kDa Dextran, which increased the medium osmolarity by 0.667mosM whereas 1%MC increases by about 0.116mosM, without changing the medium viscosity (Fig 1B). We did not observe a speed increase, implying that the observed speed increase is only the result of increased media viscosity. We also tested our observation on multiple cell lines, 3T3s, HT1080s, SUM-159s and observed a similar cell speed increase with increasing viscosity (Fig S1C, F, I). Cells also showed a phenotypic change: upon a sudden switch to high viscosity media (see Materials and Methods), there is immediately an increase in cell area in time, up to a plateau (t=30min for MDA-MB-231 cells, Fig 1F, G). MDA-MB-231 cells also travelled larger distances (mean squared displacement, or MSD) in the same amount of time in high viscosity media (Fig 1D, Fig 1C, Fig S1A, D, G). We did not observe any significant trend with changes in cell trajectory persistence, or temporal change in angular displacement (Fig S1B, E, H). This observation implies that the MSD increase is not due to cells moving more persistently in high viscosity media, compared to control media. The observed speed increase, which is measured as the magnitude of the instantaneous cell velocity, is also independent of cell persistence.

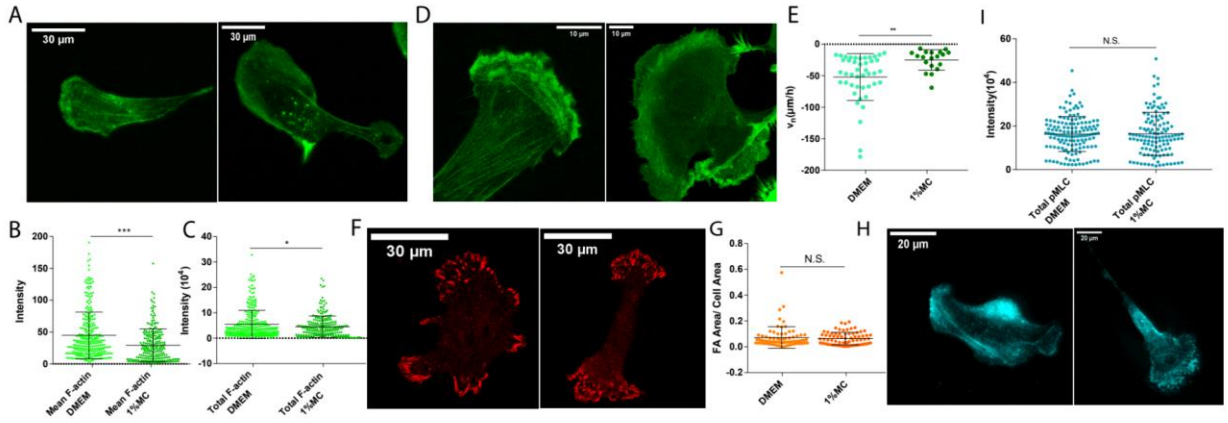

Figure 2- F-Actin dynamics and contractility in high viscous media (A) F-Actin represented by phalloidin staining, DMEM (left) and 1%MC (right) **(B), (C)** represents mean and total F-Actin comparisons of cells in DMEM (N=300) and 1%MC (N=250) **(D)** Snap of cells transfected with F-Tractin and **(E)** comparisons of retrograde flow speeds in DMEM (N=44) and 1%MC (N=19) **(F)** Vinculin staining used to quantify focal adhesions and **(G)** plot of focal adhesion density of cells in DMEM (N=74) and 1%MC (N=75) **(H)** pMLC staining DMEM (Left), 1%MC (right) **(I)** plot of total pMLC of cells in DMEM (N=142) and 1%MC (N=124).

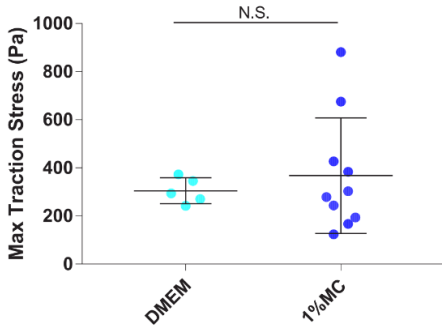

Figure S2- Traction stress comparisons (A) Traction stress plots of cells in DMEM (N=5) and 1%MC (N=10).

3.3.2 Total F-actin, focal adhesions density and phosphorylated-myosin light chain (pMLC) are unchanged while actin retrograde flow speed is reduced in high viscosity media

It is known that cell migration in 2D involves the actions of actin, contractility and focal adhesions. The active contraction generated by cells is mostly generated by myosin motors, or pMLC. We investigated the change in F-actin under the influence of high viscosity media using phalloidin staining and found no increase in total F-actin, but there is a reduction F-actin density as measured as fluorescent intensity per unit area (Fig 2B, C). This implies that F-actin is re-distributed in cells exposed to high viscosity media but increase in ECHR did not lead to a net increase of F-actin. In addition, actin retrograde flow has been found to be a key element during cell migration (Gardel et al. 2008; Swaminathan et al. 2017) and is believed to be partly driven by myosin contraction (X). Actin retrograde flow analysis yields that the retrograde flow speed reduces in high viscosity media (Fig 2D, E). However, we did not observe a change in total pMLC (Fig 2H, I) and the traction stress, as measured by traction force microscopy, did not change in high viscosity media (Fig S2).

Next we stained for the focal adhesion protein vinculin and observed that focal adhesion per unit cell area (Zinn et al. 2019) remains the same (Fig 2F, G), implying ECHR does not cause an increase in focal adhesions assembly and the speed increase cannot be attributed to increased F-Actin, pMLC, contractility or focal adhesion per unit area.

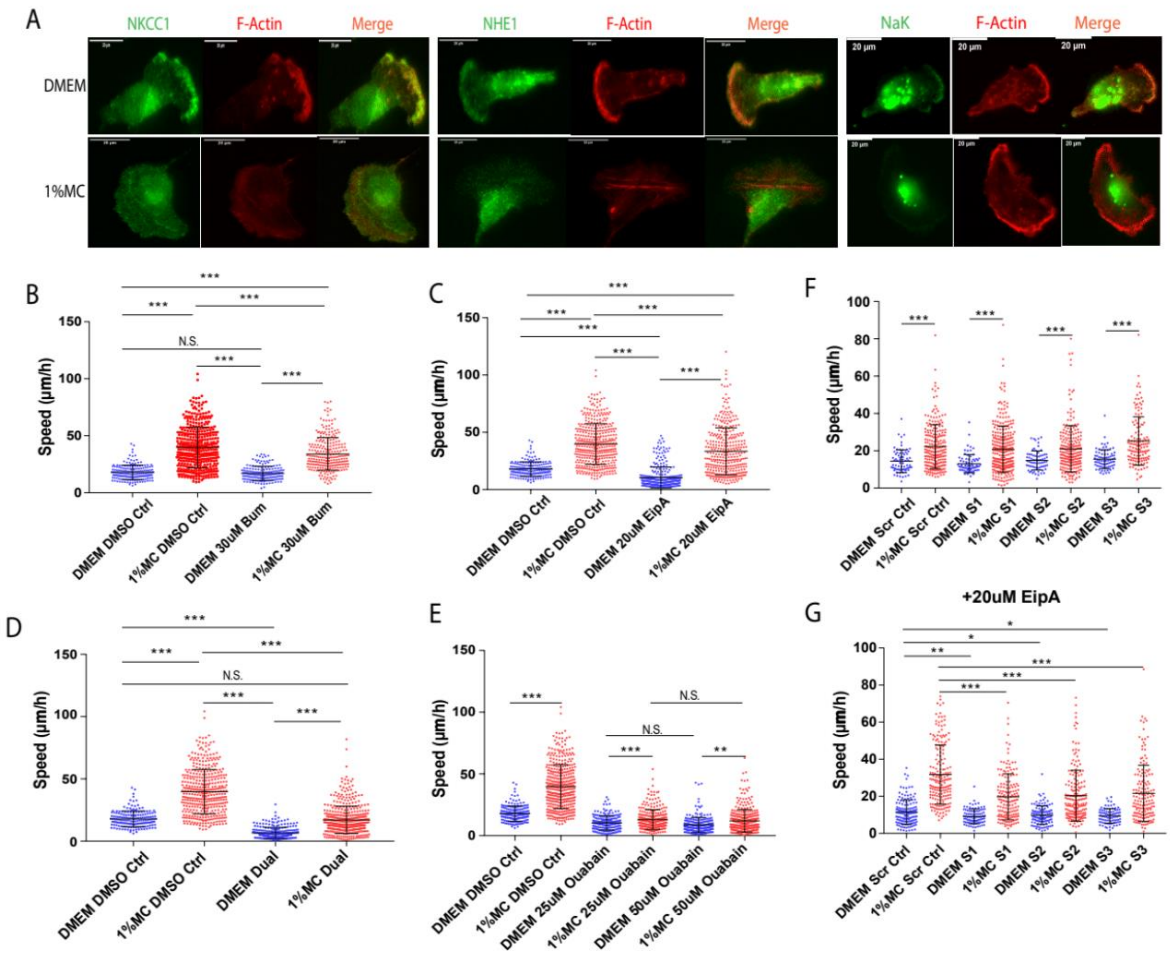

Figure 3- Influence of ion-channels on cell motility (A) Representative images of NKCC1, NHE1, NaK and F-Actin stains of cells in DMEM and 1%MC **(B)** Inhibition of NKCC1 via 30uM Bumetanide (DMEM DMSO Ctrl N=182; 1%MC DMSO Ctrl N=411; DMEM 30uM Bum N=171; 1%MC 30uM Bum N=263) **(C)** Inhibition of NHE1 via 20uM EipA (DMEM DMSO Ctrl N=182; 1%MC DMSO Ctrl N=411; DMEM 20uM EipA N=293; 1%MC 20uM EipA N=346) **(D)** Inhibition of NKCC1 and NHE1 via 30uM Bumetanide and 20uM EipA (DMEM DMSO Ctrl N=182; 1%MC DMSO Ctrl N=411; DMEM Dual N=264; 1%MC Dual N=461) (E) Inhibition of NaK via 25uM and 50uM Ouabain (DMEM DMSO Ctrl N=182; 1%MC DMSO Ctrl N=411; DMEM 25uM Ouabain N=202; 1%MC 25uM Ouabain N=288; DMEM 50uM Ouabain N=248; 1%MC 50uM Ouabain N=331) **(F)** NKCC1 Knockdown experiments (DMEM Scr Ctrl N=74; 1%MC Scr Ctrl N=224; DMEM S1 N=74; 1%MC S1 N=301; DMEM S2 N=71; 1%MC S2 N=217; DMEM S3 N=77; 1%MC S3 N=133) **(G)** Dual inhibition experiment via NKCC1 knockdown and 20uM EipA (DMEM Scr Ctrl N=148; 1%MC Scr Ctrl N=189; DMEM S1 N=93; 1%MC S1 N=166; DMEM S2 N=117; 1%MC S2 N=188; DMEM S3 N=84; 1%MC S3 N=160).

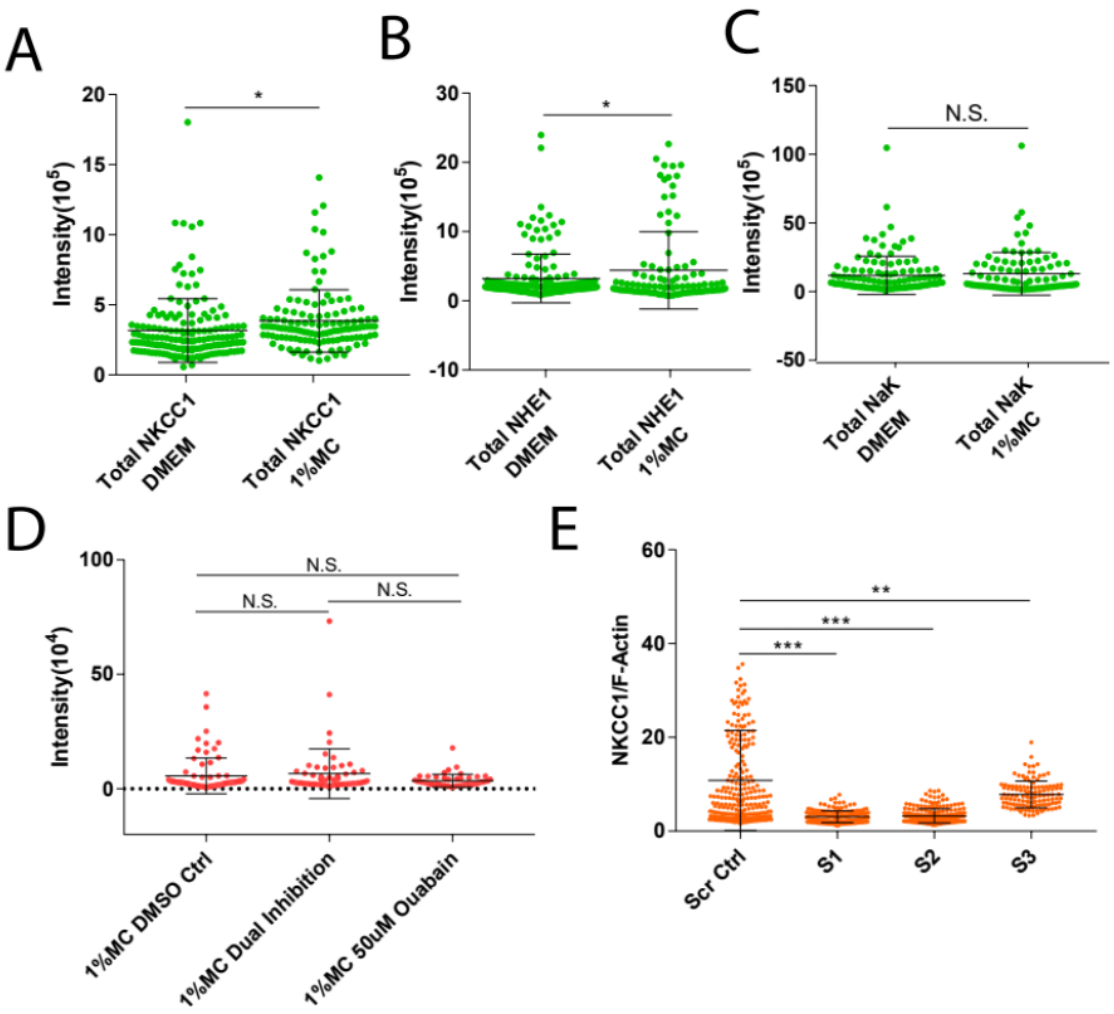

Figure S3- Total F-Actin, NKCC1, NHE1 and NaK under different conditions (A), (B) and (C) Total NKCC1 (DMEM N=157; 1%MC N=124), NHE1 (DMEM N=161; 1%MC N=106) and NaK (DMEM N=121; 1%MC N=96) of cells under no drug treatment **(D)** Total F-Actin in cells under different treatment conditions 1%MC DMSO Ctrl (N=75), 1%MC Dual inhibition (N=61), 1%MC 50uM Ouabain (N=51) **(E)** Ratio of NKCC1 to F-Actin of Control (Scr Ctrl N=240) and NKCC1 knockdowns (S1 N=185; S2 N=238; S3 N=125).

3.3.3 Water permeation plays a significant role in cell motility in viscosity media

It has been shown previously that transmembrane water flux can drive cell motility (Li and Sun 2018; Stroka et al. 2014). Furthermore, from modeling, both actin polymerization and water flux can contribute to the observed cell speed (Li et al. 2019).

In cells, transmembrane water flux is driven by ion concentration gradients across the cell membrane. These gradients are generated by ion channels and ion pumps. To investigate whether water permeation influences cell motility in high viscosity media, we performed pharmacological inhibition of ion-channel/pump NKCC1 (via Bumetanide), NHE1 (via EIPA) and NaK (via Ouabain). NKCC1 is a Na^+, K^+ and Cl^- cotransporter that plays a critical role in maintaining K^+ and Cl^- homeostasis. It has been previously implicated in cancer cell growth and motility (Cong et al. 2015; Haas and Sontheimer 2010; Zhou et al. 2017). NHE1 dictates electroneutral exchange of extracellular Na^+ and intracellular H^+ (Vallés et al. 2015). NHE1 has been shown to influence cell motility in 1D confinement (Stroka et al. 2014) and cancer metastasis (Altaf et al. 2017; Amith et al. 2017; Amith, Wilkinson, and Fliegel 2016; Amith and Fliegel 2013). We observed that inhibitions of NKCC1 and NHE1 individually does not reduce cell speed in high viscosity media. However, upon a dual inhibition, either with Bumetanide + EIPA or with NKCC1 knockdown + EIPA, there is a significant reduction in cell speed (Fig 3B, C, D, F, G; Fig S3 E), implying that NKCC1 and NHE1 in this context are functionally redundant in high viscosity media. Unlike in low viscosity media where only NHE1 inhibition can significantly impede motility, both channels can influence cell movement. When one ion pump is inhibited, cells are still able to generate Na^+ flux using the other channel.

NaK uses a single ATP molecule to pump 3 Na^+ ions out of the cell in exchange for 2 K^+ ions into the cell. NaK has been previously implicated in metastasis (Baker Bechmann et al. 2016), tumor growth (Banerjee et al. 2018) and has been used as a marker for epithelial-mesenchymal transition (EMT) in cancer and fibrosis (Rajasekaran et al. 2010). The pumping action of NaK can cause an imbalance of ions at the cell leading/trailing edge, generating water influx/efflux driven by the osmotic pressure gradient. NaK has been shown to generate water fluxes (Choudhury et al. 2019; Kennedy and Lever 1984). Upon inhibition of NaK, we observed a reduction in cell speed for both control and high viscosity media. However, the speed reduction in viscous media is more prominent (Fig 3E), implying greater contribution of ion and water fluxes in viscous microenvironments.

This conclusion is further bolstered by the fact that we did not observe a significant change in total F-Actin upon treating with either Bumetanide, EIPA or Ouabain. Lastly, we did not observe a dramatic change in the NKCC1, NHE1 or NaK expression levels in high viscosity media (Fig S3 A, B, C), implying that high viscosity media results in an intracellular re-distribution of these ion pumps.

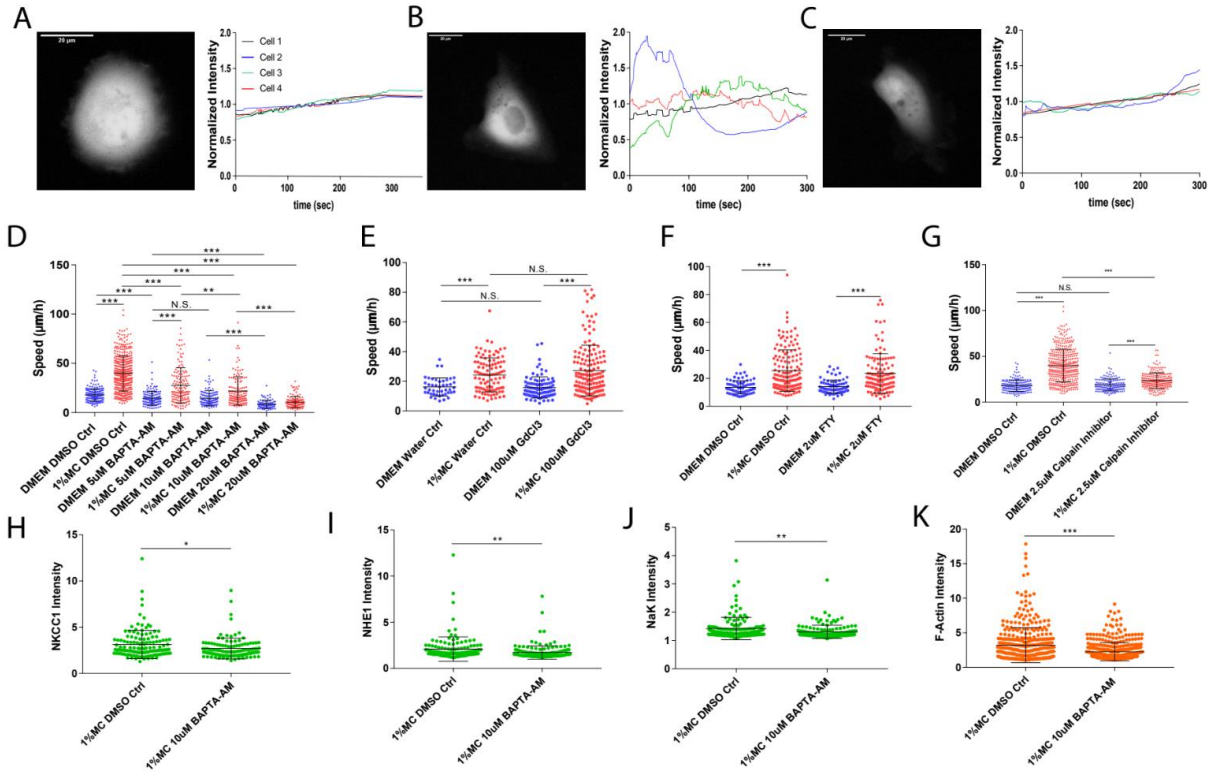

Figure 4- Investigation of Calcium (Ca^{2+}) dynamics in dictating motility (A), (B) and (C) GCamp6m transfected cells under different conditions DMEM (immediate addition), 1%MC (immediate addition) and 1%MC (long term >3hrs incubation) **(D)** Cell Speed under various levels of Ca^{2+} chelation via BAPTA-AM (DMEM DMSO Ctrl N=182; 1%MC DMSO Ctrl N=411; DMEM 5uM BAPTA-AM N=135; 1%MC 5uM BAPTA-AM N=144; DMEM 10uM BAPTA-AM N=117; 1%MC 10uM BAPTA-AM N=137; DMEM 20uM BAPTA-AM N=86; 1%MC 20uM BAPTA-AM N=127) **(E)** Non-specific inhibition of mechano-sensitive channels via $GdCl_3$ (DMEM Water Ctrl N=45; 1%MC Water Ctrl N=102; DMEM 100uM $GdCl_3$ N=96; 1%MC 100uM $GdCl_3$ N=157) **(F)** Inhibition of TRPM7 via FTY (DMEM DMSO Ctrl N=77; 1%MC DMSO Ctrl N=154; DMEM 2uM FTY N=83; 1%MC 2uM FTY N=120) **(G)** Calpain inhibition via Calpain inhibitor I (N=182; N=411; N=155; N=232) **(H), (I), (J),**

(K) Intensity ratios of NKCC1 (1%MC DMSO Ctrl N=132; 1%MC 10uM BAPTA-AM N=115), NHE1 (1%MC DMSO Ctrl N=132; 1%MC 10uM BAPTA-AM N=171), NaK (1%MC DMSO Ctrl N=133; 1%MC 10uM BAPTA-AM N=144) and F-Actin (1%MC DMSO Ctrl N=397; 1%MC 10uM BAPTA-AM N=430) of cells under Control and BAPTA-AM cases.

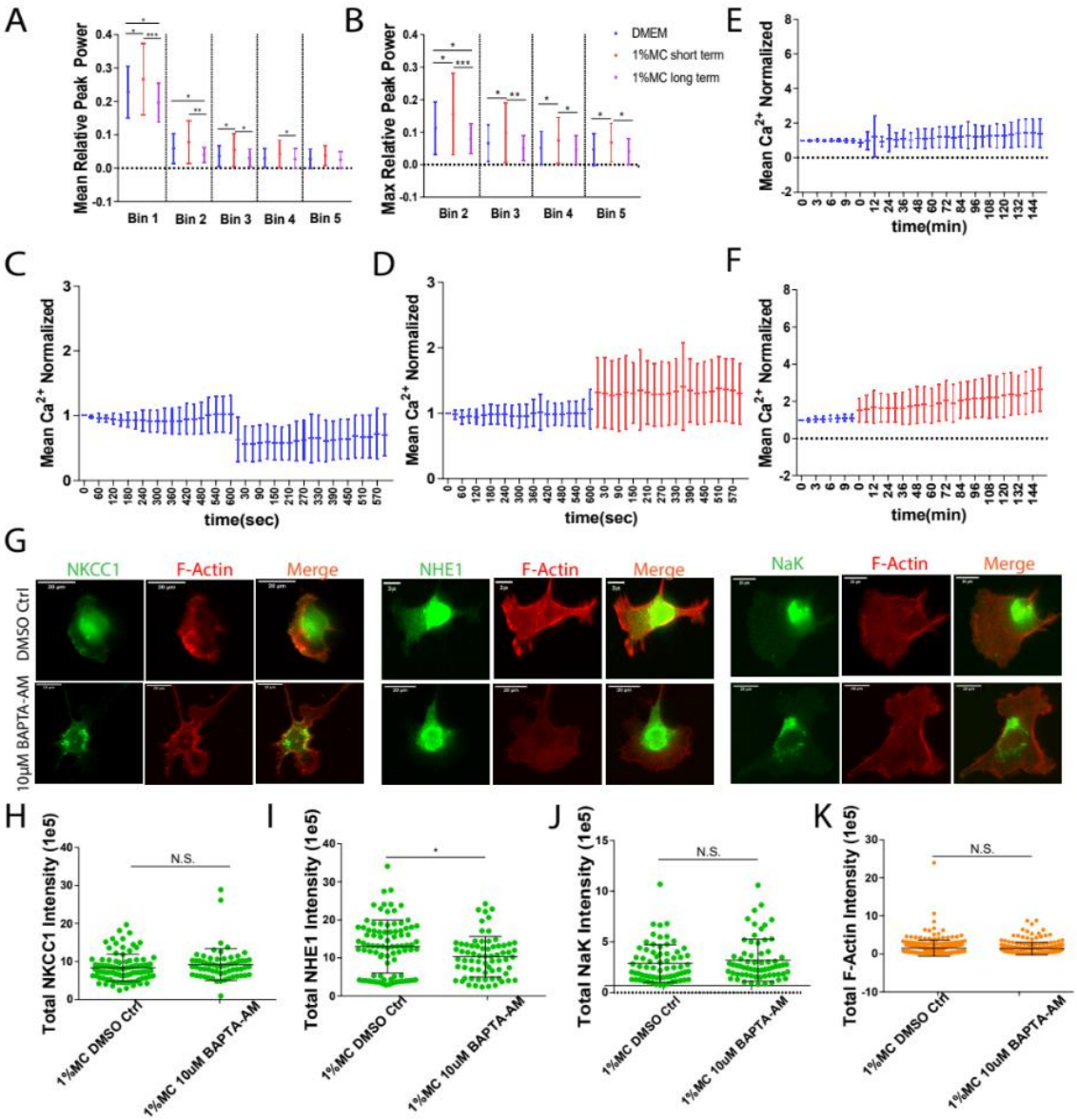

Figure S4- Quantification of Ca^{2+} dynamics of cells in normal and high viscous media (A), (B) Mean relative peak and Maximum relative peak power of cells under 3 different scenarios, namely, DMEM (immediate addition) (N=58), 1%MC (immediate addition) (N=61) and 1%MC (long term >3hrs incubation) (N=39) **(C), (D)** Ca^{2+} dynamics of cells upon immediate incubation in DMEM and 1%MC respectively over a short term (DMEM N=16; 1%MC N=29) duration (~10min) **(E), (F)** Ca^{2+} dynamics of cells upon immediate incubation in DMEM and 1%MC respectively over a long term duration (~2.5hrs) (DMEM N=20; 1%MC N=34). **(G)** Representative images of NKCC1, NHE1, NaK and F-Actin under treatment with 10uM BAPTA-AM. **(H)** Total NKCC1 1%MC DMSO Ctrl N=93; 1%MC 10uM BAPTA-AM N=62 **(I)** Total NHE1 1%MC DMSO Ctrl N=87; 1%MC 10uM BAPTA-AM N=70 **(J)** Total NaK 1%MC DMSO Ctrl N=69; 1%MC 10uM BAPTA-AM N=66 **(K)** Total F-Actin 1%MC DMSO Ctrl N=249; 1%MC 10uM BAPTA-AM N=198.

3.3.4 Calcium dynamics responds to changes in media viscosity and influence motility

Calcium (Ca^{2+}) signaling has been found to be a key component during spontaneous cell polarization and has been shown to coordinate directional cell migration (Wei et al. 2009). Cell sensing of confinement-induced ECHR is Ca^{2+} dependent and is mediated by the mechano-sensitive TRPM7 Ca^{2+} channel (Zhao et al. 2019). Moreover, mechano-sensitive Ca^{2+} channel TRPV4 has been shown to be involved in sensing mechanical compression (He et al. 2018). Ca^{2+} also has been shown to be involved in vesicle fusion reactions, stabilizing transport vesicle coats and hence dictating vesicle trafficking (Ahluwalia et al. 2001). Since Ca^{2+} also regulates fluxes of many ion channels and pumps, ion channels/pumps activity is also expected to depend on calcium. Therefore, we examined the role of Ca^{2+} in cell motility in high viscosity media by transiently transfecting cells with GCamp6M, a fluorescent live cell Ca^{2+} indicator. We observed that at short times (minutes after contact with high viscosity media), cells showed large fluctuations in Ca^{2+} levels, which ultimately plateaued after 30min (Fig 4A, B, C). Fast Fourier Transform (FFT) (UhlÈn 2004) of these signals yielded that high frequency Ca^{2+} oscillations immediately after exposure to high viscosity media, while lower frequency oscillations are observed in control media and long times after media change (Fig S4A, B). Interestingly, high viscosity media resulted in elevated levels of intracellular Ca^{2+} content, both at short and long times, compared to control media, suggesting that Ca^{2+} may a have significant role in the observed cell speed increase in high viscosity media (Fig. S4 C, D, E, F).

To perturb Ca^{2+} signaling in moving cells, we used an intracellular Ca^{2+} chelator, BAPTA-AM, and observed a significant reduction in cell speed in high viscosity media (Fig 4D). To further

investigate the role of Ca^{2+} in modulating focal adhesions, we performed calpain I & II inhibition (via calpain inhibitor I) and also found a reduction in cell speed in high viscosity media (Fig 5G). Ca^{2+} is known to activate calpain (Khorchid and Ikura 2002), which ultimately dictates focal adhesion disassembly (Franco et al. 2004).

Furthermore, BAPTA-AM caused a decrease in the leading edge localization of ion-channels such as NKCC1, NHE1 and NaK (Fig 4 H, I, J respectively) at the leading edges of cells in high viscosity media and also reduced the local F-Actin (Fig 4 K), while the total ion-channel and F-Actin content remained the same (Fig S4 G, H, I, J, K). However, non-specific inhibition of mechano-sensitive channels using $GdCl_3$, caused no dramatic reduction in speed in high viscosity media (Fig 4E) and TRPM7 inhibition does not affect cell motility in high viscosity media (Fig 4F).

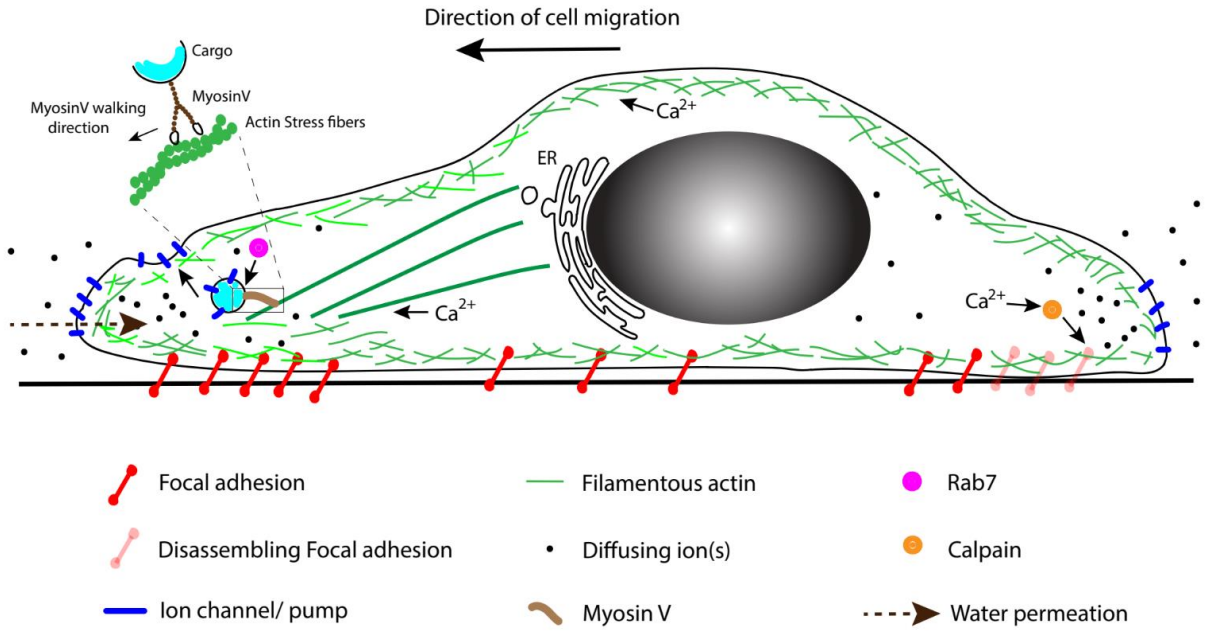

Figure 5. Schematic of the proposed mechanism of cell motility under high viscous conditions

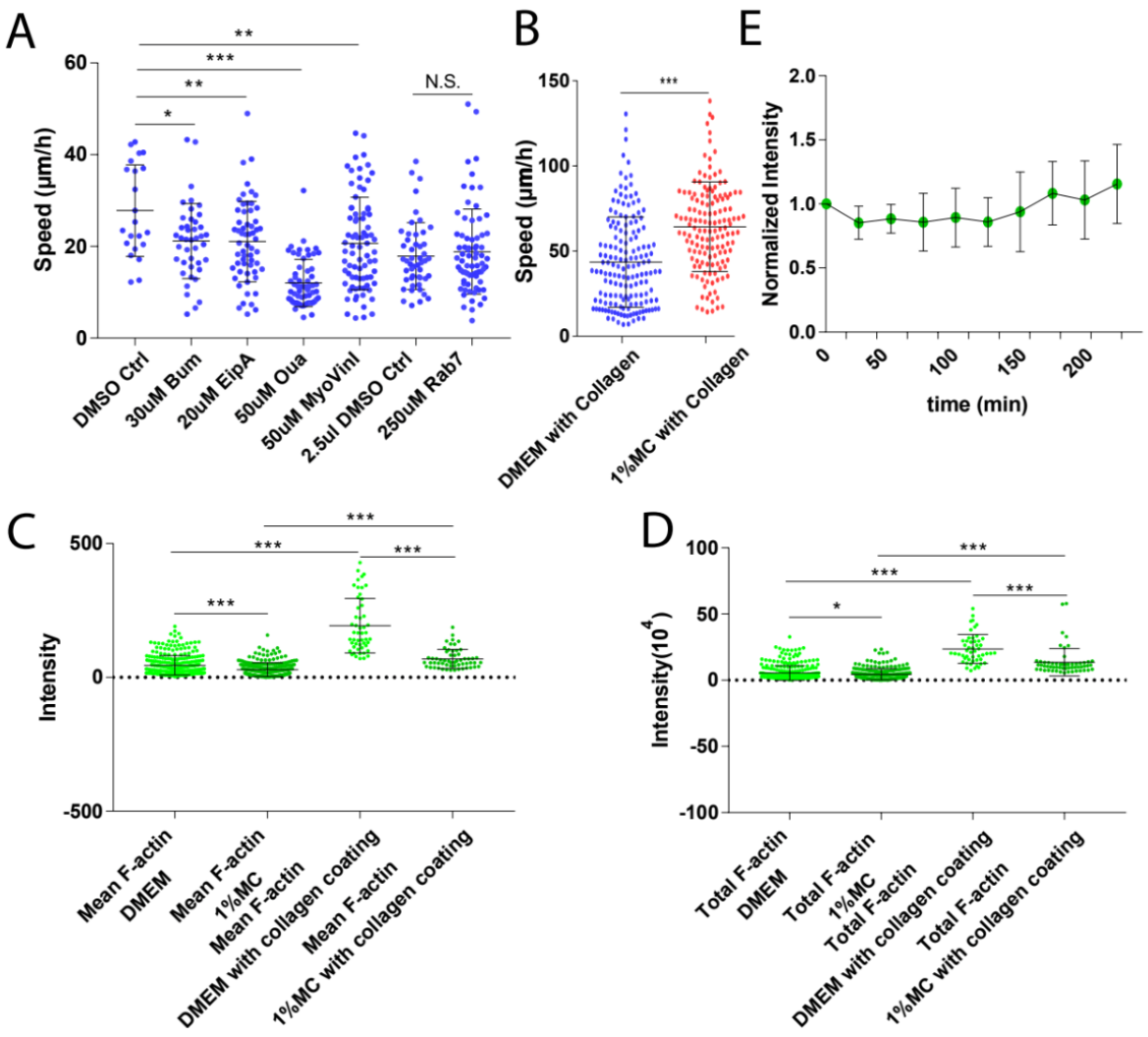

Figure S5- 3D cell speed and investigation under collagen coating (A) Cell speed in 3D under various drug treatments (DMSO Ctrl N=22; 30uM Bumetanide N=42; 20uM EipA N=59; 50uM Ouabain N=59; 50uM MyoVinI N=80; 2.5ul DMSO Ctrl N=49; 250uM C78893 N=73) **(B)** Cell speed in DMEM (N=162) and 1%MC (N=145) under 20ug/ml collagen coating **(C), (D)** Comparisons of Mean and total F-Actin of cells without [DMEM (N=300) and 1%MC (N=250)] and with 20ug/ml collagen coating [DMEM (N=51) and 1%MC (N=58)].

3.3.5 Modeling can partially explain the observed speed increase in high viscosity media

Our observed cell speed increase under higher media viscosity partially explained using a two-phase model of the cell cytoplasm (Li et al. 2019; Li and Sun 2018).

Within this model, cell boundaries can advance from both actin polymerization and water influx from exterior to the cell. When there is no water flux, the actin retrograde flow velocity is determined by the rate of actin polymerization and myosin contraction. When there is water influx, for the same rate of actin polymerization which gives the same net F-actin content remained the same (Fig. 2B, C), the model predicts that the actin retrograde flow speed is reduced. This is consistent with our observations (Fig. 2E). Model also predicts that water fluxes also increase cell speed, and the speed increase is elevated in high viscosity (or high hydraulic resistance) conditions. Our experiments show that in addition to this physical mechanism of cell speed enhancement, cells can sense the external hydraulic resistance and ion channel/pump distribution is altered in high viscosity media. The observed increase in ion channel localization to the migrating cell leading edge is probably giving rise to an increase in directional ion and water fluxes across the entire cell. An increased channel/pump polarization is expected to increase cell velocity, which has also been observed in the experiments. Modeling also predicts that cell adhesion frictional force is also an important factor in contributing to cell speed. The observed Ca^{2+} dynamics alter both ion channel distribution as well as adhesion dynamics, although no significant change in traction force, which is a measure of frictional force with the substrate, was observed (Fig. 2).

3.4 Discussion & Conclusion

By quantitatively measuring the speed of cell migration in 2D in media of different viscosity, we discovered that cells can migrate faster in media with higher viscosity. This result is unexpected since most moving objects slow down when the viscosity resistance increases. Our investigations yielded a potential mechanism that can explain the increase of cell speed under high ECHR. We found that the cell speed in high viscosity media to be a both driven by F-actin and water flux. Since water flux is primarily driven by ion fluxes across the cell surface, we investigated the role of ion-channels such as, NKCC1 and NHE1 and ion-pump, such as, NaK, in dictating motility in high viscosity media. We found that simultaneously inhibiting NKCC1 and NHE1 can decrease cell speed in higher viscosity. By impeding (LatA as well as myosin V and Rab7 inhibition) cell vesicular trafficking of these ion channels/pumps to the cell leading edge, we found that cell speed decreased significantly in high viscosity media (Fig 6).

Specifically, we observed that inhibition of actin polymerization via LatA affects the localization of all ion-channels, namely, NKCC1, NHE1 and NaK, while MyosinV inhibition has been found to affect only NKCC1 and NHE1 although to a much lesser extent (not shown in this thesis). Rab7 has been found to impede localization of just NaK although not as dramatic as the case of LatA (not shown in this thesis). This result implies that actin polymerization, although can affect actin mediated cell motility, it can also influence water permeation mediated motility mode. This result essentially links actin and water permeation mediated mode of migration through disruption of ion-channel localization at the leading edge. Furthermore, through MyosinV inhibition and Rab7 inhibtion data, we show that there does not need to be a dramatic change of total F-Actin content to bring about a difference in localization of ion-channels at the cell leading edge. Moreover, Ca^{2+} dynamics is involved in regulating motility in high viscosity. We found Ca^{2+} to play a key role in ion-channel re-distribution in high viscosity media (Fig 5). Ca^{2+} is involved in regulating ion channel trafficking and function (Li et al. 2013; Reynolds et al. 2007; Schwartz 2001). Moreover, we also observe a Ca^{2+}-dependent increase in calpain activity in high viscosity media, which could potentially change adhesion forces with the substrate (Undyala et al. 2008). It has also been observed that Focal adhesion kinase (FAK) association at focal adhesions was prolonged by Ca^{2+} and FAK auto-phosphorylation was correlated to intracellular Ca^{2+} levels, implying that Ca^{2+} can also effect focal adhesion disassembly by changing residence time of FAK at focal adhesions (Giannone et al. 2004). Furthermore, local regulation of contractile forces have been shown to be dependent on global Ca^{2+} (Doyle 2004) and local Ca^{2+} sparks allow spatial segregation of mechano-transduction events (Ellefsen et al. 2019). Quite interestingly, we found no change in the total pMLC content (in addition to focal adhesion density and traction stress) between the cases of normal and high viscous media, implying that pMLC (just like F-Actin) is redistributed all over the cell and there is no change in contractile forces involved. In depth role of contractility and focal adhesions in influencing cell motility under high viscosity conditions will require further investigation.

However, we observed that TRPM7 is not involved in changing cell speed when exposed to high viscosity media, but it is involved in sensing hydraulic resistance in confinement (Zhao et al. 2019), implying cells have different mechanisms in sensing and adapting to viscosity and geometry-mediated hydraulic resistance.

Our motility experiments are performed with glass substrates. When the substrate is coated with 20ug/ml of collagen, we also observed a cell speed increase in high viscosity media. However, this speed increase is not as dramatic as the case of no coating (Fig S5 B). With collagen coating, we found that cells contain elevated levels F-actin (Fig S5 C, D), perhaps implying that cell speed is more F-Actin driven with collagen substrates. Integrin engagement with collagen can result in RhoA activation (Gimond et al. 1999), which can result in a more actin driven motility. More studies are needed to understand how collagen ECM can change motility mechanisms.

Another key feature that might influence cell motility is the cell endocytic cycle, which allows the cell to take up external fluid, leading to forward cell movement. We have observed that EIPA(Moreau et al. 2019) inhibition of NHE1 did not cause a cell speed reduction in high viscosity media (Fig 3C). Furthermore, we performed the endocytosis experiments with 150kDa FITC Dextran and measured the mean intensity of the cell after subtracting the background and normalizing with respect to the first frame. We found that even at long time instances there is no significant endocytosis involved (Fig S5E). Since EIPA is involved in regulating micropinocytosis (Moreau et al. 2019), we conclude that the observed cell speed increase in high viscosity media is not due to elevated endocytosis which is also supported by our Dextran endocytosis data. In other situations, amoeboid cells in suspension exhibit increased endocytosis at the back and membrane trafficking from front to back (O'Neill et al. 2018). The endocytic cycle can impact cell polarization, cell area changes and membrane flow (Traynor and Kay 2007), and therefore is also as important as the cytoskeleton and ion channels in controlling cell motility. A possible role of the endocytic cycle in cell motility in high viscosity media is an important topic of future investigation.

CHAPTER 4. CONCLUSION & FUTURE WORK

4.1 Review of the findings

In this thesis, we specifically focus on studying specific mechanical elements of the tumor microenvironment (TME). We categorically demonstrate that although the biochemical factors and biochemical feedback mechanism between cancer cells and stromal cells have been studied in detail over the past, the field of mechno-chemical interactions between cancer cells and stromal cells mediated by the extracellular matrix is rather a new domain. The mechanical element investigated in this study is extracellular hydraulic resistance (ECHR).

First, we start out with an experiment-cum-modeling approach to elucidate the ECHR of a 3D matrix environment. We performed hydrostatic pressure mediated perturbation and found that rat tail type I collagen essentially demonstrates poro-elastic behavior (where at short perturbation times, the behavior is elastic while at long time instances, it behaves both as porous and elastic material). Using this model of the 3D matrix, we fit several mechanical parameters to the poro-elastic model of the collagen. Using COMSOL simulations (Paul et al. 2020; Poddar et al. 2016), we then investigated the effective hydraulic resistance faced by the cells while migrating through complex 3D space. We considered two domains, 1) 3D matrix having infinite domain 2) 3D matrix having a constrained domain. Through computational modeling we found that ECHR is a function of the viscosity of the fluid, the geometry of the object (here cell) migrating, the permeability of the matrix and the geometry of the confinement of the 3D matrix. We validate the simulations with analytical models.

Previous studies on cell migration in collagen have primarily focused on focal adhesions and the mechanical properties of the collagen (Doyle et al. 2015; Petrie and Yamada 2015). Furthermore, previous research on TME has primarily focused on the ECM mechanical properties and architecture including stiffness, alignment, crosslinking (Ahmadzadeh et al. 2017; Fraley et al. 2010). Our results show that depending on the permeability, density, and the degree of geometric confinement, moving micron-sized objects such as cells can experience substantially increased ECHR (by as much as 10^6 times) when compared to 2D micro-environments which pose a much less ECHR.

We concluded that in addition to properties such as mechanical stiffness, the fluidic environment of the cell can have an impact on cell behavior such as speed, persistence and so on.

In the next section of the thesis, I focused on studying a key mechanical element that aids ECHR, namely, viscosity. As viscosity of the extracellular fluid increases, the ECHR increases. Previously, it was believed that enhanced viscosity will result in cell speed reduction. Quite counter-intuitively we found that cell speed increases under high viscous conditions. In this section of the thesis, we propose a possible mechanism of cell speed increase under high viscous conditions (which we refer to as ECHR).

Cell migration is thought to be dominated by acto-myosin and focal adhesions (Fraley et al. 2010; Gardel et al. 2010; Sao et al. 2019; Zinn et al. 2019). Here we show that in addition to the actin driven motility, cells can also use water permeation mediated motility (Stroka et al. 2014) which was only theoretically envisioned previously (Li et al. 2019; Li and Sun 2018). Strikingly, we observed that there are no molecular changes brought about in the cell, in that, pMLC, F-Actin and Focal Adhesion density remain the same. This implies that reorganization of the proteins is an important feature of cell motility under high viscous conditions.

Through perturbation of activity/ localization of ion-channels, namely, NKCC1, NHE1 and NaK, we show that cell migration can be dramatically affected. Our results suggest a dual role of F-actin for motility in high viscosity conditions, namely, 1) it is involved in extending the cell leading edge, 2) It is also involved in directing vesicular transport and positioning of ion channels that facilitate water intake. The latter observation links actin and water permeation mediated modes of cell migration. We find that water and F-actin both contribute to the final cell speed increase observed in high viscosity environments compared to low viscous environments.

Moreover, our results show that Ca^{2+} dynamics is involved in regulating motility in high viscosity. We found Ca^{2+} to play a dominant role in ion-channel re-distribution in high viscous conditions. Ca^{2+} is not only involved in regulating ion channel trafficking and function, but also F-Actin polymerization at the leading edge of the cells.

4.2 Future work

In the work involving estimating the ECHR of a 3D matrix, we found that the effective response of the matrix is strongly dependent on the time scale of the perturbation. A significant contribution would be to actually estimate the ECHR imposed by the matrix as a single cell is migrating through the matrix. That would require estimation of the local interstitial pressure, a tool of which has been previously devised (Sao et al. 2019). Future investigations should focus not just on the mechanical aspects of the ECM, rather also consider the local fluidic environment which is the focus of this thesis. A more comprehensive approach to investigating cell motility in a TME would be to not only consider the previously well-investigated focal adhesion mediated motility (Fraley et al. 2010) but also to investigate how cells sense and respond to various cues imposed on them by the interstitial fluid, where cells can use water permeation mediated migration (Stroka et al. 2014). A unified approach towards cell migration could essentially be a significant contribution.

In the next section of the thesis, I have focused on a possible mechanism of motility under high ECHR. However, the question about how cells sense viscosity mediated ECHR still remains unanswered. It was found that TRPM7 mediates geometrical ECHR (Zhao et al. 2019). Our work hints that Rho A could be a possible viscosity sensing element, but that would require detailed investigation which is beyond the scope of this thesis. My work also hints at focal adhesion being a significant component in that, the rate of focal adhesion disassembly can govern cell migration speed under high ECHR. Closer inspection of the focal adhesion assembly/ disassembly could reveal more insights on actin mediated cell migration mode.

The endocytic cycle can influence a plethora of factors such as 1) cell polarization, 2) cell area changes and 3) membrane flow, and therefore can also be thought of as an important player as the cytoskeleton and ion channels in controlling cell motility. A possible role of the endocytic cycle in cell motility in high viscosity media is an interesting topic for future investigations.

REFERENCES

Ahluwalia, Jatinder P., Justin D. Topp, Kelly Weirather, Matthew Zimmerman, and Mark Stamnes. 2001. "A Role for Calcium in Stabilizing Transport Vesicle Coats." *Journal of Biological Chemistry* 276(36):34148–55.

Ahmadzadeh, Hossein, Marie R. Webster, Reeti Behera, Angela M. Jimenez Valencia, Denis Wirtz, Ashani T. Weeraratna, and Vivek B. Shenoy. 2017. "Modeling the Two-Way Feedback between Contractility and Matrix Realignment Reveals a Nonlinear Mode of Cancer Cell Invasion." *Proceedings of the National Academy of Sciences* 114(9):E1617–26.

Altaf, Ehtisham, Xiaoxing Huang, Jie Xiong, Xiangyong Yang, Xinzhou Deng, Meng Xiong, Lu Zhou, Shan Pan, Wen Yuan, Xinran Li, Ling Hao, Kingsley Miyanda Tembo, Ruijing Xiao, and Qiuping Zhang. 2017. "NHE1 Has a Notable Role in Metastasis and Drug Resistance of T-Cell Acute Lymphoblastic Leukemia." *Oncology Letters* 14(4):4256–62.

Amith, Schammim R., and Larry Fliegel. 2013. "Regulation of the Na+/H+ Exchanger (NHE1) in Breast Cancer Metastasis." *Cancer Research* 73(4):1259–64.

Amith, Schammim Ray, Krista Marie Vincent, Jodi Marie Wilkinson, Lynne Marie Postovit, and Larry Fliegel. 2017. "Defining the Na+/H+ Exchanger NHE1 Interactome in Triple-Negative Breast Cancer Cells." *Cellular Signalling* 29:69–77.

Amith, Schammim Ray, Jodi Marie Wilkinson, and Larry Fliegel. 2016. "Na+/H+ Exchanger NHE1 Regulation Modulates Metastatic Potential and Epithelial-Mesenchymal Transition of Triple-Negative Breast Cancer Cells." *Oncotarget* 7(16):21091–113.

An, Won G., Meera Kanekal, M. Celeste Simon, Emin Maltepe, Mikhail V Blagosklonny, and Leonard M. Neckers. 1998. "Stabilization of Wild-Type P53 by Hypoxia-Inducible Factor 1α." *Nature* 392(6674):405–8.

Antoine, Elizabeth E., Pavlos P. Vlachos, and Marissa N. Rylander. 2015. "Tunable Collagen I Hydrogels for Engineered Physiological Tissue Micro-Environments." *PLOS ONE* 10(3):e0122500.

Artym, Vira V, Stephen Swatkoski, Kazue Matsumoto, Catherine B. Campbell, Ryan J. Petrie, Emilios K. Dimitriadis, Xin Li, Susette C. Mueller, Thomas H. Bugge, Marjan Gucek, and Kenneth M. Yamada. 2015. "Dense Fibrillar Collagen Is a Potent Inducer of Invadopodia via a Specific Signaling Network." *The Journal of Cell Biology* 208(3):331—350.

Azab, Abdel Kareem, Jinsong Hu, Phong Quang, Feda Azab, Costas Pitsillides, Rana Awwad, Brian Thompson, Patricia Maiso, Jessica D. Sun, Charles P. Hart, Aldo M. Roccaro, Antonio Sacco, Hai T. Ngo, Charles P. Lin, Andrew L. Kung, Ruben D. Carrasco, Karin Vanderkerken, and Irene M. Ghobrial. 2012. "Hypoxia Promotes Dissemination of Multiple Myeloma through Acquisition of Epithelial to Mesenchymal Transition-like Features." *Blood* 119(24):5782–94.

Baker Bechmann, Marc, Deborah Rotoli, Manuel Morales, María del Carmen Maeso, María del Pino García, Julio Ávila, Ali Mobasheri, and Pablo Martín-Vasallo. 2016. "Na,K-ATPase Isozymes in Colorectal Cancer and Liver Metastases." *Frontiers in Physiology* 7(JAN):1–11.

Baker, Brendon M., and Christopher S. Chen. 2012. “Deconstructing the Third Dimension: How 3D Culture Microenvironments Alter Cellular Cues.” *Journal of Cell Science* 125(Pt 13):3015–24.

Banerjee, Moumita, Xiaoyu Cui, Zhichuan Li, Hui Yu, Liquan Cai, Xuelian Jia, Daheng He, Chi Wang, Tianyan Gao, and Zijian Xie. 2018. “Na/K-ATPase Y260 Phosphorylation–Mediated Src Regulation in Control of Aerobic Glycolysis and Tumor Growth.” *Scientific Reports* 8(1):12322.

Beck, Jennifer N., Anirudha Singh, Ashley R. Rothenberg, Jennifer H. Elisseeff, and Andrew J. Ewald. 2013. “The Independent Roles of Mechanical, Structural and Adhesion Characteristics of 3D Hydrogels on the Regulation of Cancer Invasion and Dissemination.” *Biomaterials* 34(37):9486–95.

Biot, Maurice A. 1941. “General Theory of Three-Dimensional Consolidation.” *Journal of Applied Physics* 12(2):155–64.

Bloom, Ryan J., Jerry P. George, Alfredo Celedon, Sean X. Sun, and Denis Wirtz. 2008. “Mapping Local Matrix Remodeling Induced by a Migrating Tumor Cell Using Three-Dimensional Multiple-Particle Tracking.” *Biophysical Journal* 95(8):4077–88.

Boghaert, Eline, Jason P. Gleghorn, KangAe Lee, Nikolce Gjorevski, Derek C. Radisky, and Celeste M. Nelson. 2012. “Host Epithelial Geometry Regulates Breast Cancer Cell Invasiveness.” *Proceedings of the National Academy of Sciences* 109(48):19632–37.

Casares, Laura, Romaric Vincent, Dobryna Zalvidea, Noelia Campillo, Daniel Navajas, Marino Arroyo, and Xavier Trepat. 2015. “Hydraulic Fracture during Epithelial Stretching.” *Nature Materials* 14(3):343–51.

Chen, Dongdong, Mingke Song, Osama Mohamad, and Shan Ping Yu. 2014. “Inhibition of Na+/K+-ATPase Induces Hybrid Cell Death and Enhanced Sensitivity to Chemotherapy in Human Glioblastoma Cells.” *BMC Cancer* 14(1):716.

Cheng, Alexander H. D. 2016. *Poroelasticity*. Vol. 27. Cham: Springer International Publishing.

Choudhury, Mohammad Ikbal, Yizeng Li, Panagiotis Mistriotis, Eryn E. Dixon, Debonil Maity, Rebecca Walker, Morgen Benson, Leigha Martin, Fatima Koroma, Feng Qian, Konstantinos Konstantopoulos, Owen M. Woodward, and Sean X. Sun. 2019. “Trans-Epithelial Fluid Pumping Performance of Renal Epithelial Cells and Mechanics of Cystic Expansion.”

Çinar, Yildirim. 2001. “Blood Viscosity and Blood Pressure: Role of Temperature and Hyperglycemia.” *American Journal of Hypertension* 14(5):433–38.

Cong, Damin, Wen Zhu, John S. Kuo, Shaoshan Hu, and Dandan Sun. 2015. “Ion Transporters in Brain Tumors.” *Current Medicinal Chemistry* 22(10):1171–81.

Craig, Erin M., Jonathan Stricker, Margaret Gardel, and Alex Mogilner. 2015. “Model for Adhesion Clutch Explains Biphasic Relationship between Actin Flow and Traction at the Cell Leading Edge.” *Physical Biology* 12(3):035002.

Doyle, Andrew. 2004. “Calcium Transients Induce Spatially Coordinated Increases in Traction Force during the Movement of Fish Keratocytes.” *Journal of Cell Science* 117(11):2203–14.

Doyle, Andrew D. 2016. “Generation of 3D Collagen Gels with Controlled Diverse Architectures.” Pp. 10.20.1-10.20.16 in *Current Protocols in Cell Biology*. Vol. 72. Hoboken, NJ, USA: John Wiley & Sons, Inc.

Doyle, Andrew D., Nicole Carvajal, Albert Jin, Kazue Matsumoto, and Kenneth M. Yamada. 2015. “Local 3D Matrix Microenvironment Regulates Cell Migration through Spatiotemporal Dynamics of Contractility-Dependent Adhesions.” *Nature Communications* 6:8720.

Durning, Patricia, and S. .. Schor. 1984. “Fibroblasts From Patients With Breast Cancer Show Abnormal Migratory Behaviour in Vitro.” *The Lancet* 324(8408):890–92.

Durst, Franz. n.d. *Fluid Mechanics- An Introduction to the Theory of Fluid Flows*. Springer Berlin Heidelberg.

Ellefsen, Kyle L., Jesse R. Holt, Alice C. Chang, Jamison L. Nourse, Janahan Arulmoli, Armen H. Mekhdjian, Hamid Abuwarda, Francesco Tombola, Lisa A. Flanagan, Alexander R. Dunn, Ian Parker, and Medha M. Pathak. 2019. “Myosin-II Mediated Traction Forces Evoke Localized Piezo1-Dependent Ca2+ Flickers.” *Communications Biology* 2(1):298.

Erler, Janine T., Kevin L. Bennewith, Monica Nicolau, Nadja Dornhöfer, Christina Kong, Quynh-Thu Le, Jen-Tsan Ashley Chi, Stefanie S. Jeffrey, and Amato J. Giaccia. 2006. “Lysyl Oxidase Is Essential for Hypoxia-Induced Metastasis.” *Nature* 440(7088):1222–26.

Even-Ram, Sharona, and Kenneth M. Yamada. 2005. “Cell Migration in 3D Matrix.” *Current Opinion in Cell Biology* 17(5):524–32.

Ferreira, Lino S., Sharon Gerecht, Jason Fuller, Hester F. Shieh, Gordana Vunjak-Novakovic, and Robert Langer. 2007. “Bioactive Hydrogel Scaffolds for Controllable Vascular Differentiation of Human Embryonic Stem Cells.” *Biomaterials* 28(17):2706–17.

Fraley, Stephanie I., Yunfeng Feng, Ranjini Krishnamurthy, Dong-Hwee Kim, Alfredo Celedon, Gregory D. Longmore, and Denis Wirtz. 2010. “A Distinctive Role for Focal Adhesion Proteins in Three-Dimensional Cell Motility.” *Nature Cell Biology* 12(6):598–604.

Franco, Santos J., Mary A. Rodgers, Benjamin J. Perrin, Jaewon Han, David A. Bennin, David R. Critchley, and Anna Huttenlocher. 2004. “Calpain-Mediated Proteolysis of Talin Regulates Adhesion Dynamics.” *Nature Cell Biology* 6(10):977–83.

Fratzl, P. n.d. “Collagen: Structure and Mechanics, an Introduction.” Pp. 1–13 in *Collagen*. Boston, MA: Springer US.

Furukawa, Koji, Takeo Abumiya, Keiji Sakai, Miki Hirano, Toshiya Osanai, Hideo Shichinohe, Naoki Nakayama, Ken Kazumata, Toshimitsu Aida, and Kiyohiro Houkin. 2016. “Measurement of Human Blood Viscosity by an Electromagnetic Spinning Sphere Viscometer.” *Journal of Medical Engineering & Technology* 40(6):285–92.

Gaggioli, Cedric, Steven Hooper, Cristina Hidalgo-Carcedo, Robert Grosse, John F. Marshall, Kevin Harrington, and Erik Sahai. 2007. “Fibroblast-Led Collective Invasion of Carcinoma Cells with Differing Roles for RhoGTPases in Leading and Following Cells.” *Nature Cell Biology* 9(12):1392–1400.

Gardel, Margaret L., Benedikt Sabass, Lin Ji, Gaudenz Danuser, Ulrich S. Schwarz, and Clare M. Waterman. 2008. “Traction Stress in Focal Adhesions Correlates Biphasically with Actin Retrograde Flow Speed.” *Journal of Cell Biology* 183(6):999–1005.

Gardel, Margaret L., Ian C. Schneider, Yvonne Aratyn-Schaus, and Clare M. Waterman. 2010. "Mechanical Integration of Actin and Adhesion Dynamics in Cell Migration." *Annual Review of Cell and Developmental Biology* 26(1):315–33.

Gautieri, Alfonso, Simone Vesentini, Alberto Redaelli, and Markus J. Buehler. 2012. "Viscoelastic Properties of Model Segments of Collagen Molecules." *Matrix Biology : Journal of the International Society for Matrix Biology* 31(2):141–49.

Gerecht, Sharon, Jason A. Burdick, Lino S. Ferreira, Seth A. Townsend, Robert Langer, and Gordana Vunjak-Novakovic. 2007. "Hyaluronic Acid Hydrogel for Controlled Self-Renewal and Differentiation of Human Embryonic Stem Cells." *Proceedings of the National Academy of Sciences* 104(27):11298 LP – 11303.

Giannone, Grégory, Philippe Rondé, Mireille Gaire, Joël Beaudouin, Jacques Haiech, Jan Ellenberg, and Kenneth Takeda. 2004. "Calcium Rises Locally Trigger Focal Adhesion Disassembly and Enhance Residency of Focal Adhesion Kinase at Focal Adhesions." *Journal of Biological Chemistry* 279(27):28715–23.

Gimond, Clotilde, Arjan van der Flier, Sanne van Delft, Cord Brakebusch, Ingrid Kuikman, John G. Collard, Reinhard Fässler, and Arnoud Sonnenberg. 1999. "Induction of Cell Scattering by Expression of B1 Integrins in B1-Deficient Epithelial Cells Requires Activation of Members of the Rho Family of Gtpases and Downregulation of Cadherin and Catenin Function." *The Journal of Cell Biology* 147(6):1325–40.

Gjorevski, Nikolce, and Celeste M. Nelson. 2012. "Mapping of Mechanical Strains and Stresses around Quiescent Engineered Three-Dimensional Epithelial Tissues." *Biophysical Journal* 103(1):152–62.

Gkretsi, Vasiliki, and Triantafyllos Stylianopoulos. 2018. "Cell Adhesion and Matrix Stiffness: Coordinating Cancer Cell Invasion and Metastasis." *Frontiers in Oncology* 8:145.

Gonzalez-Molina, Jordi, Xiaoli Zhang, Michela Borghesan, Joana Mendonça da Silva, Maooz Awan, Barry Fuller, Núria Gavara, and Clare Selden. 2018. "Extracellular Fluid Viscosity Enhances Liver Cancer Cell Mechanosensing and Migration." *Biomaterials* 177:113–24.

Grabmaier, Karin, Mirjam C. A de Weijert, Gerald W. Verhaegh, Jack A. Schalken, and Egbert Oosterwijk. 2004. "Strict Regulation of CAIX(G250/MN) by HIF-1alpha in Clear Cell Renal Cell Carcinoma." *Oncogene* 23(33):5624–31.

Guo, K., G. Searfoss, D. Krolikowski, M. Pagnoni, C. Franks, K. Clark, K. T. Yu, M. Jaye, and Y. Ivashchenko. 2001. "Hypoxia Induces the Expression of the Pro-Apoptotic Gene BNIP3." *Cell Death and Differentiation* 8(4):367–76.

Haas, Brian R., and Harald Sontheimer. 2010. "Inhibition of the Sodium-Potassium-Chloride Cotransporter Isoform-1 Reduces Glioma Invasion." *Cancer Research* 70(13):5597–5606.

Han, Weijing, Shaohua Chen, Wei Yuan, Qihui Fan, Jianxiang Tian, Xiaochen Wang, Longqing Chen, Xixiang Zhang, Weili Wei, Ruchuan Liu, Junle Qu, Yang Jiao, Robert H. Austin, and Liyu Liu. 2016. "Oriented Collagen Fibers Direct Tumor Cell Intravasation." *Proceedings of the National Academy of Sciences of the United States of America* 113(40):11208–13.

He, Lijuan, Jiaxiang Tao, Debonil Maity, Fangwei Si, Yi Wu, Tiffany Wu, Vishnu Prasath, Denis Wirtz, and Sean X. Sun. 2018. "Role of Membrane-Tension Gated Ca2+ Flux in Cell Mechanosensation." *Journal of Cell Science* 131(4):jcs208470.

Huber, Deborah, Ali Oskooei, Xavier Casadevall i Solvas, Andrew deMello, and Govind V Kaigala. 2018. “Hydrodynamics in Cell Studies.” *Chemical Reviews* 118(4):2042–79.
Hutson, Heather N., Taylor Marohl, Matthew Anderson, Kevin Eliceiri, Paul Campagnola, and Kristyn S. Masters. 2016. “Calcific Aortic Valve Disease Is Associated with Layer-Specific Alterations in Collagen Architecture.” *PLOS ONE* 11(9):e0163858.
Iliopoulos, O., A. P. Levy, C. Jiang, W. G. Jr Kaelin, and M. A. Goldberg. 1996. “Negative Regulation of Hypoxia-Inducible Genes by the von Hippel-Lindau Protein.” *Proceedings of the National Academy of Sciences of the United States of America* 93(20):10595–99.
Iyer, N. V, L. E. Kotch, F. Agani, S. W. Leung, E. Laughner, R. H. Wenger, M. Gassmann, J. D. Gearhart, A. M. Lawler, A. Y. Yu, and G. L. Semenza. 1998. “Cellular and Developmental Control of O2 Homeostasis by Hypoxia-Inducible Factor 1 Alpha.” *Genes & Development* 12(2):149–62.
Jansen, Karin A., Albert J. Licup, Abhinav Sharma, Robbie Rens, Fred C. MacKintosh, and Gijsje H. Koenderink. 2018. “The Role of Network Architecture in Collagen Mechanics.” *Biophysical Journal* 114(11):2665–78.
Jeffery, P. K. 2001. “Remodeling in Asthma and Chronic Obstructive Lung Disease.” *American Journal of Respiratory and Critical Care Medicine* 164(10 Pt 2):S28-38.
Jiang, Si. Tse., Woei. Jer. Chuang, and Ming. Jer. Tang. 2000. “Role of Fibronectin Deposition in Branching Morphogenesis of Madin-Darby Canine Kidney Cells.” *Kidney International* 57(5):1860–67.
Kalluri, Raghu. 2016. “The Biology and Function of Fibroblasts in Cancer.” *Nature Reviews Cancer* 16(9):582–98.
Kennedy, Brian G., and Julia E. Lever. 1984. “Regulation of Na+, K+-ATPase Activity in MDCK Kidney Epithelial Cell Cultures: Role of Growth State, Cyclic AMP, and Chemical Inducers of Dome Formation and Differentiation.” *Journal of Cellular Physiology* 121(1):51–63.
Khorchid, Ahmad, and Mitsuhiko Ikura. 2002. “How Calpain Is Activated by Calcium.” *Nature Structural Biology* 9(4):239–41.
Kilic-Eren, Mehtap, Tulin Boylu, and Vedrana Tabor. 2013. “Targeting PI3K/Akt Represses Hypoxia Inducible Factor-1α Activation and Sensitizes Rhabdomyosarcoma and Ewing’s Sarcoma Cells for Apoptosis.” *Cancer Cell International* 13(1):36.
Kim, Deok-Ho, Paolo P. Provenzano, Chris L. Smith, and Andre Levchenko. 2012. “Matrix Nanotopography as a Regulator of Cell Function.” *Journal of Cell Biology* 197(3):351–60.
Krishnamachary, Balaji, Shannon Berg-Dixon, Brian Kelly, Faton Agani, David Feldser, Gloria Ferreira, Narayan Iyer, Jessica LaRusch, Brian Pak, Panthea Taghavi, and Gregg L. Semenza. 2003. “Regulation of Colon Carcinoma Cell Invasion by Hypoxia-Inducible Factor 1.” *Cancer Research* 63(5):1138–43.
Krishnamachary, Balaji, David Zagzag, Hideko Nagasawa, Karin Rainey, Hiroaki Okuyama, Jin H. Baek, and Gregg L. Semenza. 2006. “Hypoxia-Inducible Factor-1-Dependent Repression of E-Cadherin in von Hippel-Lindau Tumor Suppressor-Null Renal Cell Carcinoma Mediated by TCF3, ZFHX1A, and ZFHX1B.” *Cancer Research* 66(5):2725–31.

Levental, Kandice R., Hongmei Yu, Laura Kass, Johnathon N. Lakins, Mikala Egeblad, Janine T. Erler, Sheri F. T. Fong, Katalin Csiszar, Amato Giaccia, Wolfgang Weninger, Mitsuo Yamauchi, David L. Gasser, and Valerie M. Weaver. 2009. "Matrix Crosslinking Forces Tumor Progression by Enhancing Integrin Signaling." *Cell* 139(5):891–906.

Li, Xiuju, Daniel Prins, Marek Michalak, and Larry Fliegel. 2013. "Calmodulin-Dependent Binding to the NHE1 Cytosolic Tail Mediates Activation of the Na + /H + Exchanger by Ca 2+ and Endothelin." *American Journal of Physiology-Cell Physiology* 305(11):C1161–69.

Li, Yizeng, and Sean X. Sun. 2018. "Transition from Actin-Driven to Water-Driven Cell Migration Depends on External Hydraulic Resistance." *Biophysical Journal* 114(12):2965–73.

Li, Yizeng, Lingxing Yao, Yoichiro Mori, and Sean X. Sun. 2019. "On the Energy Efficiency of Cell Migration in Diverse Physical Environments." *Proceedings of the National Academy of Sciences* 116(48):23894–900.

Licup, Albert James, Stefan Münster, Abhinav Sharma, Michael Sheinman, Louise M. Jawerth, Ben Fabry, David A. Weitz, and Fred C. MacKintosh. 2015. "Stress Controls the Mechanics of Collagen Networks." *Proceedings of the National Academy of Sciences of the United States of America* 112(31):9573–78.

Liu, Fei, Justin D. Mih, Barry S. Shea, Alvin T. Kho, Asma S. Sharif, Andrew M. Tager, and Daniel J. Tschumperlin. 2010. "Feedback Amplification of Fibrosis through Matrix Stiffening and COX-2 Suppression." *The Journal of Cell Biology* 190(4):693–706.

de Lucas, Beatriz, Laura M. Pérez, and Beatriz G. Gálvez. 2017. "Importance and Regulation of Adult Stem Cell Migration." *Journal of Cellular and Molecular Medicine* 22(2):746–54.

Ma, Haiwen, Tao Li, Zhennan Tao, Long Hai, Luqing Tong, Li Yi, Iruni R. Abeysekera, Peidong Liu, Yang Xie, Jiabo Li, Feng Yuan, Chen Zhang, Yihan Yang, Haolang Ming, Shengping Yu, and Xuejun Yang. 2019. "NKCC1 Promotes EMT-like Process in GBM via RhoA and Rac1 Signaling Pathways." *Journal of Cellular Physiology* 234(2):1630–42.

Maity, Debonil, Aditya Bandopadhyay, and Suman Chakraborty. 2016. "Rheology Modulated Non-Equilibrium Fluctuations in Time-Dependent Diffusion Processes." *Physica A: Statistical Mechanics and Its Applications* 462:654–66.

Maity, Debonil, Yizeng Li, Yun Chen, and Sean X. Sun. 2019. "Response of Collagen Matrices under Pressure and Hydraulic Resistance in Hydrogels." *Soft Matter* 15(12):2617–26.

Mason, Brooke N., Alina Starchenko, Rebecca M. Williams, Lawrence J. Bonassar, and Cynthia A. Reinhart-King. 2013. "Tuning Three-Dimensional Collagen Matrix Stiffness Independently of Collagen Concentration Modulates Endothelial Cell Behavior." *Acta Biomaterialia* 9(1):4635–44.

Mathieu, Véronique, Christine Pirker, Elisabeth Martin de Lassalle, Mathieu Vernier, Tatjana Mijatovic, Nancy DeNeve, Jean-François Gaussin, Mischael Dehoux, Florence Lefranc, Walter Berger, and Robert Kiss. 2009. "The Sodium Pump Alpha1 Sub-Unit: A Disease Progression-Related Target for Metastatic Melanoma Treatment." *Journal of Cellular and Molecular Medicine* 13(9B):3960–72.

Mierke, Claudia Tanja. 2019. “The Matrix Environmental and Cell Mechanical Properties Regulate Cell Migration and Contribute to the Invasive Phenotype of Cancer Cells.” *Reports on Progress in Physics* 82(6):064602.

Miron-Mendoza, Miguel, Joachim Seemann, and Frederick Grinnell. 2010. “The Differential Regulation of Cell Motile Activity through Matrix Stiffness and Porosity in Three Dimensional Collagen Matrices.” *Biomaterials* 31(25):6425–35.

Mohammadi, Hamid, Pamma D. Arora, Craig A. Simmons, Paul A. Janmey, and Christopher A. McCulloch. 2015. “Inelastic Behaviour of Collagen Networks in Cell-Matrix Interactions and Mechanosensation.” *Journal of the Royal Society, Interface* 12(102):20141074.

Moreau, Hélène D., Carles Blanch-Mercader, Rafaele Attia, Mathieu Maurin, Zahraa Alraies, Doriane Sanséau, Odile Malbec, Maria-Graciela Delgado, Philippe Bousso, Jean-François Joanny, Raphaël Voituriez, Matthieu Piel, and Ana-Maria Lennon-Duménil. 2019. “Macropinocytosis Overcomes Directional Bias in Dendritic Cells Due to Hydraulic Resistance and Facilitates Space Exploration.” *Developmental Cell* 49(2):171-188.e5.

Muz, Barbara, Pilar de la Puente, Feda Azab, and Abdel Kareem Azab. 2015. “The Role of Hypoxia in Cancer Progression, Angiogenesis, Metastasis, and Resistance to Therapy.” *Hypoxia* 83.

Nam, Sungmin, Kenneth H. Hu, Manish J. Butte, and Ovijit Chaudhuri. 2016. “Strain-Enhanced Stress Relaxation Impacts Nonlinear Elasticity in Collagen Gels.” *Proceedings of the National Academy of Sciences of the United States of America* 113(20):5492–97.

Nguyen-Ngoc, Kim-Vy, Kevin J. Cheung, Audrey Brenot, Eliah R. Shamir, Ryan S. Gray, William C. Hines, Paul Yaswen, Zena Werb, and Andrew J. Ewald. 2012. “ECM Microenvironment Regulates Collective Migration and Local Dissemination in Normal and Malignant Mammary Epithelium.” *Proceedings of the National Academy of Sciences of the United States of America* 109(39):E2595-604.

Nguyen-Ngoc, Kim-Vy, Eliah R. Shamir, Robert J. Huebner, Jennifer N. Beck, Kevin J. Cheung, and Andrew J. Ewald. 2015. “3D Culture Assays of Murine Mammary Branching Morphogenesis and Epithelial Invasion.” *Methods in Molecular Biology (Clifton, N.J.)* 1189:135–62.

O’Neill, Patrick R., Jean A. Castillo-Badillo, Xenia Meshik, Vani Kalyanaraman, Krystal Melgarejo, and N. Gautam. 2018. “Membrane Flow Drives an Adhesion-Independent Amoeboid Cell Migration Mode.” *Developmental Cell* 46(1):9-22.e4.

Paget, S. 1989. “The Distribution of Secondary Growths in Cancer of the Breast. 1889.” *Cancer Metastasis Reviews* 8(2):98–101.

Paul, Rajorshi, Debonil Maity, Pranshu Agarwal, Aditya Bandopadhyay, and Suman Chakraborty. 2020. “Electrokinetics of Non-Newtonian Fluids in Poly-Electrolyte Grafted Nanochannels: Effects of Ion-Partitioning and Confinement.” *Journal of Non-Newtonian Fluid Mechanics* 104348.

Petrie, Ryan J., and Kenneth M. Yamada. 2012. “At the Leading Edge of Three-Dimensional Cell Migration.” *Journal of Cell Science* 125(24):5917–26.

Petrie, Ryan J., and Kenneth M. Yamada. 2015. “Fibroblasts Lead the Way: A Unified View of 3D Cell Motility.” *Trends in Cell Biology* 25(11):666–74.

Poddar, Antarip, Debonil Maity, Aditya Bandopadhyay, and Suman Chakraborty. 2016. "Electrokinetics in Polyelectrolyte Grafted Nanofluidic Channels Modulated by the Ion Partitioning Effect." *Soft Matter* 12(27):5968–78.

Pointer, Kelli B., Paul A. Clark, Alexandra B. Schroeder, M. Shahriar Salamat, Kevin W. Eliceiri, and John S. Kuo. 2017. "Association of Collagen Architecture with Glioblastoma Patient Survival." *Journal of Neurosurgery* 126(6):1812–21.

Polacheck, William J., Joseph L. Charest, and Roger D. Kamm. 2011. "Interstitial Flow Influences Direction of Tumor Cell Migration through Competing Mechanisms." *Proceedings of the National Academy of Sciences* 108(27):11115 LP – 11120.

Pollard, Thomas D., and Gary G. Borisy. 2003. "Cellular Motility Driven by Assembly and Disassembly of Actin Filaments." *Cell* 112(4):453–65.

Prentice-Mott, Harrison V, Chi-Han Chang, L. Mahadevan, Timothy J. Mitchison, Daniel Irimia, and Jagesh V Shah. 2013. "Biased Migration of Confined Neutrophil-like Cells in Asymmetric Hydraulic Environments." *Proceedings of the National Academy of Sciences* 110(52):21006 LP – 21011.

Provenzano, Paolo P., David R. Inman, Kevin W. Eliceiri, Justin G. Knittel, Long Yan, Curtis T. Rueden, John G. White, and Patricia J. Keely. 2008. "Collagen Density Promotes Mammary Tumor Initiation and Progression." *BMC Medicine* 6:11.

Provenzano, Paolo P., David R. Inman, Kevin W. Eliceiri, Steven M. Trier, and Patricia J. Keely. 2008. "Contact Guidance Mediated Three-Dimensional Cell Migration Is Regulated by Rho/ROCK-Dependent Matrix Reorganization." *Biophysical Journal* 95(11):5374–84.

Rajasekaran, S. A., Thu P. Huynh, Daniel G. Wolle, Cromwell E. Espineda, Landon J. Inge, Anna Skay, Charles Lassman, Susanne B. Nicholas, Jeffrey F. Harper, Anna E. Reeves, Mansoor M. Ahmed, James M. Leatherman, James M. Mullin, and Ayyappan K. Rajasekaran. 2010. "Na,K-ATPase Subunits as Markers for Epithelial-Mesenchymal Transition in Cancer and Fibrosis." *Molecular Cancer Therapeutics* 9(6):1515–24.

Raub, Christopher B., Vinod Suresh, Tatiana Krasieva, Julia Lyubovitsky, Justin D. Mih, Andrew J. Putnam, Bruce J. Tromberg, and Steven C. George. 2007. "Noninvasive Assessment of Collagen Gel Microstructure and Mechanics Using Multiphoton Microscopy." *Biophysical Journal* 92(6):2212–22.

Ray, Arja, Oscar Lee, Zaw Win, Rachel M. Edwards, Patrick W. Alford, Deok-Ho Kim, and Paolo P. Provenzano. 2017. "Anisotropic Forces from Spatially Constrained Focal Adhesions Mediate Contact Guidance Directed Cell Migration." *Nature Communications* 8(1):14923.

Ray, Arja, Zachary M. Slama, Rachel K. Morford, Samantha A. Madden, and Paolo P. Provenzano. 2017. "Enhanced Directional Migration of Cancer Stem Cells in 3D Aligned Collagen Matrices." *Biophysical Journal* 112(5):1023–36.

Repke, Kurt R. H. 1988. "The Role of the Na+/K+ Pump in Normal and Cancer Cell Proliferation." Pp. 160–76 in *Biomembranes*. Berlin, Heidelberg: Springer Berlin Heidelberg.

Reynolds, Amy, Alyson Parris, Luke A. Evans, Susanne Lindqvist, Paul Sharp, Michael Lewis, Richard Tighe, and Mark R. Williams. 2007. “Dynamic and Differential Regulation of NKCC1 by Calcium and CAMP in the Native Human Colonic Epithelium.” *The Journal of Physiology* 582(2):507–24.

Riching, Kristin M., Benjamin L. Cox, Max R. Salick, Carolyn Pehlke, Andrew S. Riching, Susan M. Ponik, Benjamin R. Bass, Wendy C. Crone, Yi Jiang, Alissa M. Weaver, Kevin W. Eliceiri, and Patricia J. Keely. 2014. “3D Collagen Alignment Limits Protrusions to Enhance Breast Cancer Cell Persistence.” *Biophysical Journal* 107(11):2546–58.

Roberts, Andrew M., Ian R. Watson, Andrew J. Evans, David A. Foster, Meredith S. Irwin, and Michael Ohh. 2009. “Suppression of Hypoxia-Inducible Factor 2 Restores P53 Activity via Hdm2 and Reverses Chemoresistance of Renal Carcinoma Cells.” *Cancer Research* 69(23):9056–64.

Roselli, Robert J., and Kenneth R. Diller. 2011. *Biotransport: Principles and Applications*. Vol. 58. edited by Intergovernmental Panel on Climate Change. New York, NY: Springer New York.

Sao, Kimheak, Tia M. Jones, Andrew D. Doyle, Debonil Maity, Galina Schevzov, Yun Chen, Peter W. Gunning, and Ryan J. Petrie. 2019. “Myosin II Governs Intracellular Pressure and Traction by Distinct Tropomyosin-Dependent Mechanisms” edited by C. Parent. *Molecular Biology of the Cell* 30(10):1170–81.

Schmidt, A., and O. F. Weber. 2006. “In Memoriam of Rudolf Virchow: A Historical Retrospective Including Aspects of Inflammation, Infection and Neoplasia.” Pp. 1–15 in *Infection and Inflammation: Impacts on Oncogenesis*. Vol. 13. Basel: KARGER.

Schwartz, Arnold. 2001. “The Importance of Calcium in Interpretation of NaK-ATPase Isoform Function in the Mouse Heart.” *Cardiovascular Research* 51(1):9–12.

Semenza, G L. 2013. “Cancer–Stromal Cell Interactions Mediated by Hypoxia-Inducible Factors Promote Angiogenesis, Lymphangiogenesis, and Metastasis.” *Oncogene* 32(35):4057–63.

Semenza, Gregg L. 2013. “HIF-1 Mediates Metabolic Responses to Intratumoral Hypoxia and Oncogenic Mutations.” *Journal of Clinical Investigation* 123(9):3664–71.

Shao, Danying, Herbert Levine, and W. J. Rappel. 2012. “Coupling Actin Flow, Adhesion, and Morphology in a Computational Cell Motility Model.” *Proceedings of the National Academy of Sciences* 109(18):6851–56.

Shen, Zhilei Liu, Harold Kahn, Roberto Ballarini, and Steven J. Eppell. 2011. “Viscoelastic Properties of Isolated Collagen Fibrils.” *Biophysical Journal* 100(12):3008–15.

Shiozaki, Atsushi. 2014. “Role of the Na + /K + /2Cl - Cotransporter NKCC1 in Cell Cycle Progression in Human Esophageal Squamous Cell Carcinoma.” *World Journal of Gastroenterology* 20(22):6844.

Siemeister, G., K. Weindel, K. Mohrs, B. Barleon, G. Martiny-Baron, and D. Marmé. 1996. “Reversion of Deregulated Expression of Vascular Endothelial Growth Factor in Human Renal Carcinoma Cells by von Hippel-Lindau Tumor Suppressor Protein.” *Cancer Research* 56(10):2299–2301.

Siemens, D. Robert, Nianping Hu, Abdol Karim Sheikhi, Eugene Chung, Lisa J. Frederiksen, Hugh Pross, and Charles H. Graham. 2008. “Hypoxia Increases Tumor Cell Shedding of MHC Class I Chain-Related Molecule: Role of Nitric Oxide.” *Cancer Research* 68(12):4746–53.

Simpson, Craig D., Imtiaz A. Mawji, Kika Anyiwe, Moyo A. Williams, Xiaoming Wang, Amudha L. Venugopal, Marcela Gronda, Rose Hurren, Sonia Cheng, Stefano Serra, Reza Beheshti Zavareh, Alessandro Datti, Jeffrey L. Wrana, Shereen Ezzat, and Aaron D. Schimmer. 2009. “Inhibition of the Sodium Potassium Adenosine Triphosphatase Pump Sensitizes Cancer Cells to Anoikis and Prevents Distant Tumor Formation.” *Cancer Research* 69(7):2739–47.

Sitkovsky, Michail V. 2009. “T Regulatory Cells: Hypoxia-Adenosinergic Suppression and Re-Direction of the Immune Response.” *Trends in Immunology* 30(3):102–8.

Staller, Peter, Jitka Sulitkova, Joanna Lisztwan, Holger Moch, Edward J. Oakeley, and Wilhelm Krek. 2003. “Chemokine Receptor CXCR4 Downregulated by von Hippel-Lindau Tumour Suppressor PVHL.” *Nature* 425(6955):307–11.

Stein, Andrew M., David A. Vader, David A. Weitz, and Leonard M. Sander. 2011. “The Micromechanics of Three-Dimensional Collagen-I Gels.” *Complexity* 16:22–28.

Stroka, Kimberly M., Hongyuan Jiang, Shih-Hsun Chen, Ziqiu Tong, Denis Wirtz, Sean X. Sun, and Konstantinos Konstantopoulos. 2014. “Water Permeation Drives Tumor Cell Migration in Confined Microenvironments.” *Cell* 157(3):611–23.

Sundararaghavan, Harini G., Gary A. Monteiro, Norman A. Lapin, Yves J. Chabal, Jennifer R. Miksan, and David I. Shreiber. 2008. “Genipin-Induced Changes in Collagen Gels: Correlation of Mechanical Properties to Fluorescence.” *Journal of Biomedical Materials Research. Part A* 87(2):308–20.

Swaminathan, Vinay, Joseph Mathew Kalappurakkal, Shalin B. Mehta, Pontus Nordenfelt, Travis I. Moore, Nobuyasu Koga, David A. Baker, Rudolf Oldenbourg, Tomomi Tani, Satyajit Mayor, Timothy A. Springer, and Clare M. Waterman. 2017. “Actin Retrograde Flow Actively Aligns and Orients Ligand-Engaged Integrins in Focal Adhesions.” *Proceedings of the National Academy of Sciences* 114(40):10648–53.

Traynor, David, and Robert R. Kay. 2007. “Possible Roles of the Endocytic Cycle in Cell Motility.” *Journal of Cell Science* 120(14):2318–27.

Trepat, Xavier, Zaozao Chen, and Ken Jacobson. 2012. “Cell Migration.” Pp. 139–48 in *Comprehensive Physiology*. Vol. 176. Hoboken, NJ, USA: John Wiley & Sons, Inc.

van Uden, Patrick, Niall S. Kenneth, and Sonia Rocha. 2008. “Regulation of Hypoxia-Inducible Factor-1α by NF-KB.” *Biochemical Journal* 412(3):477–84.

UhlÈn, Per. 2004. *Spectral Analysis of Calcium Oscillations*.

Undyala, Vishnu V, Micah Dembo, Katherine Cembrola, Benjamin J. Perrin, Anna Huttenlocher, John S. Elce, Peter A. Greer, Y. -l. Wang, and Karen A. Beningo. 2008. “The Calpain Small Subunit Regulates Cell-Substrate Mechanical Interactions during Fibroblast Migration.” *Journal of Cell Science* 121(21):3581–88.

Vallés, Patricia G., Victoria Bocanegra, Andrea Gil Lorenzo, and Valeria Victoria Costantino. 2015. “Physiological Functions and Regulation of the Na+/H+ Exchanger [NHE1] in Renal Tubule Epithelial Cells.” *Kidney and Blood Pressure Research* 40(5):452–66.

Vicente-Manzanares, Miguel. 2005. “Cell Migration at a Glance.” *Journal of Cell Science* 118(21):4917–19.

Wei, Chaoliang, Xianhua Wang, Min Chen, Kunfu Ouyang, Long-Sheng Song, and Heping Cheng. 2009. “Calcium Flickers Steer Cell Migration.” *Nature* 457(7231):901–5.

Wirtz, Denis, Konstantinos Konstantopoulos, and Peter C. Searson. 2011. “The Physics of Cancer: The Role of Physical Interactions and Mechanical Forces in Metastasis.” *Nature Reviews Cancer* 11(7):512–22.

Wisdom, Katrina M., Kolade Adebowale, Julie Chang, Joanna Y. Lee, Sungmin Nam, Rajiv Desai, Ninna Struck Rossen, Marjan Rafat, Robert B. West, Louis Hodgson, and Ovijit Chaudhuri. 2018. “Matrix Mechanical Plasticity Regulates Cancer Cell Migration through Confining Microenvironments.” *Nature Communications* 9(1):4144.

Wong, Andrew D., and Peter C. Searson. 2014. “Live-Cell Imaging of Invasion and Intravasation in an Artificial Microvessel Platform.” *Cancer Research* 74(17):4937 LP – 4945.

Wu, Pei-Hsun, Daniele M. Gilkes, and Denis Wirtz. 2018. “The Biophysics of 3D Cell Migration.” *Annual Review of Biophysics* 47(1):549–67.

Yamada, Kenneth M., and Michael Sixt. 2019. “Mechanisms of 3D Cell Migration.” *Nature Reviews Molecular Cell Biology* (Box 1).

Zagzag, David, Balaji Krishnamachary, Herman Yee, Hiroaki Okuyama, Luis Chiriboga, M. Aktar Ali, Jonathan Melamed, and Gregg L. Semenza. 2005. “Stromal Cell–Derived Factor-1α and CXCR4 Expression in Hemangioblastoma and Clear Cell-Renal Cell Carcinoma: Von Hippel-Lindau Loss-of-Function Induces Expression of a Ligand and Its Receptor.” *Cancer Research* 65(14):6178–88.

Zanotelli, Matthew R., Zachary E. Goldblatt, Joseph P. Miller, Francois Bordeleau, Jiahe Li, Jacob A. VanderBurgh, Marsha C. Lampi, Michael R. King, and Cynthia A. Reinhart-King. 2018. “Regulation of ATP Utilization during Metastatic Cell Migration by Collagen Architecture.” *Molecular Biology of the Cell* 29(1):1–9.

Zhao, Runchen, Alexandros Afthinos, Tian Zhu, Panagiotis Mistriotis, Yizeng Li, Selma A. Serra, Yuqi Zhang, Christopher L. Yankaskas, Shuyu He, Miguel A. Valverde, Sean X. Sun, and Konstantinos Konstantopoulos. 2019. “Cell Sensing and Decision-Making in Confinement: The Role of TRPM7 in a Tug of War between Hydraulic Pressure and Cross-Sectional Area.” *Science Advances* 5(7):eaaw7243.

Zhou, Yaya, Wei Sun, Ning Chen, Chen Xu, Xinxin Wang, Kun Dong, Binxue Zhang, Jian Zhang, Ning Hao, Aihua Sun, Handong Wei, Fuchu He, and Ying Jiang. 2017. “Discovery of NKCC1 as a Potential Therapeutic Target to Inhibit Hepatocellular Carcinoma Cell Growth and Metastasis.” *Oncotarget* 8(39):66328–42.

Zinn, Ashtyn, Silvia M. Goicoechea, Gabriel Kreider-Letterman, Debonil Maity, Sahezeel Awadia, Luis Cedeno-Rosario, Yun Chen, and Rafael Garcia-Mata. 2019. “The Small GTPase RhoG Regulates Microtubule-Mediated Focal Adhesion Disassembly.” *Scientific Reports* 9(1):5163.

CURRICULUM VITAE

Debonil Maity

Baltimore, Maryland, United States
(+1)6673038725
debonilmaity@gmail.com
https://www.linkedin.com/in/debonil-maity-873b8956/

Summary

- Researcher with an entrepreneurial mindset, with 5+ years of experience in initiating and managing projects, resulting in 4 cross-institutional collaborations, 11 journal publications, 13 conference presentations and 8 awards.
- Demonstrated strong leadership skills, adaptability and commercial acumen by leading an interdisciplinary team of 4 graduate students and 1 post-doctoral fellow to strategize a business plan for a medical device.
- Demonstrated ability to identify key problem statements amid ambiguity and execute pertinent ideas in a high pressure scenario by managing 3+ parallel projects.

Work Experience

Project Management (as Graduate Research Assistant) Aug 2015-present
Johns Hopkins University, USA

- Demonstrated effective teamwork, collaboration and pressure management skills by managing 10+ multi-faceted projects related to cancer cell metastasis and tumor microenvironment, resulting in numerous publications and awards.
- Demonstrated excellent communication skills by presenting research findings at several prestigious conferences and seminars with audiences of about 100.
- Have 4+ years of experience in Confocal, Epifluorescence, DIC and Phase Contrast microscopy.
- Trained more than 10 high school, undergraduate and graduate students on conducting scientific research and usage of scientific instruments or software packages and conducted market research to procure pertinent products and instruments related to immunofluorescence and microscopy, demonstrating product and market knowledge.
- Have working knowledge of Phase I-IV Clinical Trials and compliance with ICH GCP.

Research Internship May 2013-July 2013
University of Alberta, Canada

- Performed Brownian dynamics and Monte Carlo simulations to elucidate the motion of particles in an opto-electric trap, demonstrating strong analytical abilities.
- Collaborated with 3 research groups and communicated my findings to an audience of about 30 at the University of Alberta Research Experience Seminar.

Education

Chemical and Biomolecular Engineering PhD Aug 2015-present
Johns Hopkins University, Baltimore, MD, USA
Mechanical Engineering BS, MS April 2010-May 2015
Indian Institute of Technology (IIT), Kharagpur, WB, India

Techniques, Software and Skills

MATLAB	Project Management	Relationship building
3D cell culture	COMSOL	Critical thinking
Microfabrication	ImageJ	Decision making
Microfluidics	Microsoft Office	Strategic planning
Microscopy	FORTRAN	Conflict resolution
Cancer Biology		
Transfection		
Traction Force Microscopy		

Affiliations & Awards

- Member, American Society for Cell Biology, ASCB 2016- present
- Member, Biophysical Society, BPS 2019
- Travel Awards, ASCB Annual Meetings 2016 and 2017
- Invited Talk, ASCB Annual Meeting 2017
- Travel Award, US National Academy of Engineering 2017
- Tiara Foundation Special Grant 2015
- Charpak Internship Scholarship 2014
- Indian Academy of Sciences Fellowship 2013
- University of Alberta Research Experience 2013